A dual function for the chromatin organizer Special A-T rich Binding Protein 1 in B-lineage cells

Morgane Thomas, Charlotte Bruzeau, Ophélie Alyssa Martin, Justine Pollet, Sébastien Bender, Claire Carrion, Sandrine Le Noir, Eric Pinaud

A dual function for the chromatin organizer Special A-T rich Binding Protein 1 in B-lineage cells

Morgane Thomas 1£, Charlotte Bruzeau 1, Ophélie Alyssa Martin 1, Justine Pollet 1, Sébastien Bender 1,2,3, Claire Carrion 1, Sandrine Le Noir 1‡ and Eric Pinaud 1‡

1 Laboratoire Contrôle de la Réponse Immune B et des Lymphoprolifération (CRIBL), Université de Limoges, CNRS Unité Mixte de Recherche 7276, Inserm Unité 1262, Limoges, France.

2 Centre Hospitalier Universitaire Dupuytren, Service d'Immunopathologie, Limoges, France.

3 Centre Hospitalier Universitaire de Limoges, Centre National de l'Amylose AL et Autres Maladies par Dépôt d'Immunoglobulines Monoclonales, Limoges, France.

£ Current Address : Laboratoire Suivi des Thérapies Innovantes, Institut de Génétique Humaine, UMR 9002 CNRS-UM, Montpellier, France

‡ corresponding authors

Correspondence should be addressed to: eric.pinaud@unilim.fr and sandrine.le-noir@unilim.fr

Keywords: B cells, nuclear factor, ambivalent, somatic hypermutation

Abstract

SATB1 (Special A-T rich Binding protein 1) is a cell type specific factor that regulates the genetic network in developing T cells and neurons. In T cells, SATB1 is required for lineage commitment, VDJ recombination, development and maturation. Considering that its expression varies during B cell differentiation, the involvement of SATB1 needed to be clarified in this lineage. Using a KO mouse model deleting SATB1 from the pro-B cell stage, we examined the consequences of SATB1 deletion in naive and activated B cell subsets. Our model indicates firstly, unlike its essential function in T cells, that SATB1 is dispensable for B cell development and the establishment of a broad IgH repertoire. Second, we show that SATB1 exhibits an ambivalent function in mature B cells, acting sequentially as a positive and negative regulator of Ig gene transcription in naive and activated cells, respectively. Third, our study indicates that the negative regulatory function of SATB1 in B cells extends to the germinal center response in which this factor limits somatic hypermutation of Ig genes.

Introduction

The transcription factor Special A-T rich binding protein 1 (SATB1) is a factor able to bind to Matrix Attachment Regions (MAR) in the nucleus [1]. This MAR-binding protein (MAR-BP) is indispensable for T lymphocyte development [2–4] through its implication in properly organizing nuclear architecture, especially chromatin folding [5–7]. Murine SATB1, sharing more than 98% identity with its human homologue, can multimerize through an ubiquitin-like domain [8] and interacts with chromatin through its CUT-like and homeodomains respectively involved in DNA binding affinity and specificity [9,10]. One historic feature of SATB1 is its ability to tie nuclear matrix proteins [11,12]. Another essential feature, as a transcription factor, is its capacity to bind DNA for gene regulation. Strikingly, such interactions were found to occur in nucleosome-dense regions, preferentially at AT-rich sequences in the nucleosomal core [13], a feature that strongly supports its candidacy as a pioneer factor. Given its multivalent potency as a nuclear matrix scaffolding factor, a genome organizer involved in chromatin looping and a transcription factor, the exact mechanism linking this MAR-BP to gene regulation remains puzzling. The large body of literature related to SATB1 in T cells suggest that this factor is capable of flexible functions; either binding to euchromatin [5,6] or nucleosome-dense regions [13], depending on the cell type and development stage assessed. Long distance interactions between promoters and enhancers can be promoted by SATB1 homotetramerization [8]. A negative regulatory function for SATB1 was attributed to its capacity to recruit chromatin modifiers such as Histone deacetylase 1 (HDAC1) [14]. Indeed, SATB1 is subject to posttranslational modification: phosphorylation of this MAR-BP modifies interactions with chromatin corepressor and coactivator complexes, leading to a switch in its transcriptional activity [15,16]; SATB1 acetylation disrupts its interaction with C-terminal binding protein 1 (CtBP1) [17]. Moreover, regulation of *Satb1* gene is by itself tightly regulated in T cells by interchanging promoter usage, resulting in fine tuning of protein expression [18,19]. These multiple levels of regulation suggest the need for meticulous control of SATB1 expression.

SATB1 deletion models in the mouse led to major alterations in neuronal, hematopoietic and immune systems [2,20] and pointed out broad and critical functions for this protein in mouse development. SATB1 is a major player in early hematopoiesis since it promotes hematopoietic stem cell self-renewal (HSC) [21]. Based on its relative expression level in differentiating HSC [22], SATB1 favors the lymphoid lineage [23]. In erythrocyte and myeloid cells, this protein also modulates epigenetic marks by association with CBP (CREB binding protein) to control β-globin and NADPH oxydase gene expression [24–26]. There is also growing evidence showing that SATB1 is involved in cancer and auto-immune diseases [6,7,27,28] highlighting the necessity to decipher its regulation in immune cells.

Due to thymus alteration in *Satb1* KO mice [2], SATB1's functions were largely studied in T-cells. Initially described as a repressor factor [12,29], SATB1 proved to be also a transcriptional activator

[6,30]. As an example of ambivalence, SATB1 could repress *c-myc* in resting T-cells while stimulating its expression in activated T cells [3]. It is now established that this MAR BP is a major regulator of thymocyte development throughout all differentiation stages from progenitors to regulatory subsets [28,31,32]. One notable role of SATB1 in T cells is its activator function for *Rag* gene expression in order to promote VDJ recombination and shape the T cell receptor repertoire [33,34]. In this context, SATB1 has been shown to bridge *Rag1* and *Rag2* gene promoters and the distant antisilencer element (ASE) of this locus[33].

By contrast to the vast knowledge on SATB1 fine tuning and regulatory functions in T lymphocytes, little is known on the potency of SATB1 to regulate B cell development, beyond HSC fate decision [22,23]. Initial studies reported a discrete defect on B cell numbers in *Satb1* KO mice [2]. Taking advantage of its elegant fluorescent reporter model, Yokota group's described fluctuations in *Satb1* expression throughout B cell development with higher expression in naive B cell subsets. In this study authors proposed that SATB1 is involved in BCR-mediated B cell survival [35]. Many aspects of the literature point to a potential function for SATB1 during B cell development. Given its regulatory function for *Rag* gene expression in T cells [33], the potential implication of SATB1 in V(D)J recombination of Ig genes in B cells needs to be examined. Moreover, since SATB1 was discovered by its ability to bind the $MAR_{E\mu}$ region of the *IgH* locus [1], we could postulate a role for SATB1 in Ig heavy chain expression.

In this study, we examined SATB1 implication in B-lineage cell development and depicted its critical function on immunoglobulin production using a conditional KO mouse model allowing deletion of this factor in B-lineage cells. Although we found SATB1 nonessential for B cell development, we showed that this factor displays an ambivalent function in late developing B cell subsets: acting sequentially as a positive and then negative regulator of Ig gene transcription. The negative regulatory function of SATB1 extends to the germinal center reaction in which this factor limits Ig gene somatic hypermutation.

Materials and Methods

Mice: *Satb1*$^{tm1a/wt}$ mice come from the Mouse Clinical Institute (MCI) (IR00004167/ P4167). First crossings with 129S4/SvJae-*Gt(ROSA)26Sor*$^{tm2(FLP*)sor}$/J mice (The Jackson Laboratory) removed reporter and marker cassette placed between *Frt* sites. Second crossings with B6.C(CG)-*Cd79a*$^{tm1(cre)Reth}$/EhobJ mice (The Jackson Laboratory) deleted *Satb1-exon4* due to CRE recombinase expression in B-lineage cells [36]. *Aicda*$^{-/-}$ homozygous mice (kindly provided by Pr. T. Honjo) were used to prepare control samples devoid of SHM, as reported in [37]. All experiments, excepted 3C-HTGTS, were performed on two-month-old mice. Primers used for genotyping are listed in *Supplementary* Table S1. All animal strains were bred and maintained in SPF conditions at 21–23°C with a 12-h light/dark cycle. Procedures were reviewed and approved by the Ministère de l'Enseignement Supérieur, de la Recherche et de l'Innovation APAFIS#16639-2018090612249522v2.

Western Blot: B cells from spleen were sorted with EASYSEP MOUSE B cell isolation kit (Stem Cell Technologies) and lysed using RIPA buffer (Santa Cruz) completed with protease inhibitor (Orthovanadate, PMSF, anti-protease cocktail). Proteins were quantified with Pierce BCA Protein Assay kit (Thermo Scientific) and denatured 5 minutes at 95°C. TGX Stain-free FastCast 12% acrylamide gels (Bio-Rad Laboratories) were used to separate proteins that were transferred on Transblot Turbo polyvinylidene fluoride membranes (Bio-Rad laboratories) with Transblot Turbo Transfer System. After blocking incubation with Phosphate Buffer Saline (PBS)- 5% skim milk, SATB1 primary antibody was incubated overnight at 4°C. Membrane was incubated with secondary antibody with PBS-3% milk. Proteins were detected and quantified with PIERCE ECL Western Blotting Substrate (Thermo Scientific) and ChemiDoc Touch Imaging System coupled to Image Lab J6.0 software (Bio-Rad Laboratories). Antibodies and concentrations used are in *Supplementary* Table S2. Unprocessed raw data are provided in *Supplementary* Fig. S1*A*)

Enzyme-linked ImmunoSorbent Assay (ELISA): Sera were collected from the blood of two-month-old mice. Supernatants were obtained after sorting B cells from spleens and *in vitro* LPS-activation during 4 days. Plates were coated overnight with 1µg/ml of primary antibody Goat Anti-Mouse Unlabeled IgM, IgG3, IgG1 or IgA (Southern Biotech) diluted in sodium carbonate buffer. Plates were blocked with PBS-3% bovine serum albumin 1 hour at 37°C. Supernatant or diluted sera were incubated 2 hours at 37°C then secondary antibody conjugated with alkaline phosphatase (Southern Biotech) was incubated 1 hour at 37°C. Enzymatic reaction was performed by adding SigmaFast™ p-nitrophenyl phosphate tablet. DO were measured at 405 nm on Thermo scientific MULTISKAN FC. Antibodies and concentrations used are in *Supplementary* Table S2.

Flow Cytometry: To analyze B cell populations, spleen and bone marrow were collected, crushed and filtered through Clearline Streaner 40 µm (Fisherbrand); lymphocyte numbers were quantified in a Cell-Dyn Emerald counter (Abbott). Cell suspensions were labeled in FACS Buffer (PBS buffer (Eurobio), 10% BSA (Stem Cell Technologies) 2mM EDTA) containing antibodies for 20 minutes at 4°C and analyzed on BD LSRFortessa SORP flow cytometer (BD Bioscience). For intracellular staining, cells were first stained for surface markers. After washing, cells were treated with the fixation/permeabilization kit Intraprep (Beckman Coulter, A07803), following the manufacturer's instructions. Mean Fluorescence Intensity values were normalized to WT values; antibodies used are provided in *Supplementary* Table S2. Gating strategies to evaluate proportions and numbers of B cell subsets are provided in *Supplementary* Fig. S1.

RNA extraction: Pre-B cells, splenic resting B cells, *in vitro*-activated cells with LPS for 2 or 4 days, plasma cells and GC B cells were lyzed with TRIZOL Reagent (Ambion Life Technologies) and RNA extraction was done following recommendations of DirectZol RNA microprep kit (ZymoResearch).

RT-qPCR: 1µg RNA from B cell subset samples was treated with DNase I Amplification Grade (Invitrogen) and reverse transcription was done following the High Capacity cDNA Reverse Transcription kit protocol (Applied Biosystem). Quantitative PCR was performed on 20ng cDNA using either SensiFAST Probe Hi-ROX or SensiFAST SYBR Hi-ROX kits (BioLine) on a Quant Studio III (Applied BioSystem). *IgH* and *Igk* primary transcripts were quantified as previously described [38]. *Satb1* transcripts were measured by TaqMan assays with Mm.PT.58.13287891 (IDT), *Rag 1* and *Rag 2* transcripts with Mm01270936_m1 and Mm00501300_m1 (ThermoFisher), respectively. Transcript quantification was carried out with normalization to *Hprt* (Mm.PT.58.32092191 - IDT) for resting and *in vitro*-stimulated cells, and to *B220* (Mm.PT.58.32086646 - IDT) for GC B cells. Specific primers designed to amplify membrane and secreted *Igµ* transcripts, as well as *Sµ* transcripts are listed in *Supplementary* Table S1.

Repertoire: Pre-B cells from bone marrow were enriched using mouse CD25 MicroBead Kit (Miltenyi Biotec). Library preparation was adapted from methods previously described[39,40]. Transcripts were amplified by 5'RACE PCR using reverse primer hybridizing within *µ* gene and Cap race primer carrying Unique Molecular Identifiers (UMIs). ProtoScript® II (New England Biolabs, Ipswich, MA) was used for reverse transcription and amplicons were obtained using Phusion® High Fidelity DNA Polymerase (New England Biolabs, Ipswich, MA) according to the manufacturer's instructions. (Primers are listed in *Supplementary* Table S1). Illumina adapter and tag sequences were added by primer extension[42]. Resulting libraries were sequenced on Illumina MiSeq sequencing system using MiSeq Reagent kit V3 600 cycles. Paired reads were merged as

previously described[42] and UMIs were treated with MIGEC software. Repertoire analysis was done using IMGT/HIGHV-QUEST online tool (http://imgt.org/) [43].

In vitro Stimulation: Splenic B cells isolated with EASYSEP MOUSE B cell isolation kit (Stem Cell Technologies) were cultured at $1x10^6$ cells/ mL in RPMI 1640 medium (Eurobio) supplemented with 10% fetal bovine serum (Dutscher), 2mM Glutamine (Eurobio), 1% Eagle's Non Essential Amino Acids (Eurobio), 50U/ml of penicillin-streptomycin (Gibco), 1mM sodium pyruvate (Eurobio), 129 µM 2-βmercaptoethanol (Sigma-Aldrich) in the presence of 1µg/ml Lipopolysaccharide (LPS-Invivogen). An aliquot of cells was collected for analysis and sample preparation at day 2 or 4 after stimulation. Same isolation protocol and cell culture reagents were used for Anti-CD40 + IL4 in vitro stimulation by replacing LPS with 5µg/ml of anti-CD40 antibody (R&D Systems, listed in *Supplementary* Table S2).and 20ng/mL recombinant mouse IL4 (Peprotech). An aliquot of cells was collected for analysis and sample preparation at day 3 and 4 after stimulation.

In vitro Ethynil-DeoxyUridine (EdU) Incorporation: Splenic B cells were cultured as described above and EdU was added 48 hours later and incorporated for 24 hours. Cells were then processed by following recommendations of Click-it EdU Alexa Fluor 488 Flow Cytometry Assay Kit (Thermo Fisher Scientific). EdU incorporation was evaluated by flow cytometry on BD LSRFortessa SORP flow cytometer (BD Bioscience)

NP-CGG immunization: Nitrophenylacetyl-Chicken Gamma Globulin (NP-CGG) immunization was realized by injecting 100µg NP-CGG (N-5055C-5 Biosearch Technologies) precipitated with complete for the first intraperitoneal injection (day 0) and incomplete Freund's adjuvant for the second one at day 12. Pre-immune sera were collected before day 0 and immunized sera were collected at days 8 and 17. Mice were sacrificed at day 17 and splenic GC B cells were sorted to extract DNA for SHM quantification by HTS.

Cell sorting: Plasma cells from spleen or plasmablasts from *in vitro* stimulation were sorted using B220 and CD138 surface markers on BD FACS ARIA III (BD Bioscience). GC B cells were sorted using B220 and GL7 cell surface markers (*Supplementary* Table S2).

Somatic Hypermutation Analysis: SHM analysis was performed on $B220^+/GL7^+$ GG B cells sorted from Peyer's patches or immunized spleens from *wt*, *Satb1* cKO and *Aicda* KO mice. 5'*Sµ*, 3'J_H4 and 3'*Jκ5* intronic regions were amplified from 10,000 cells with specific primers (listed in *Supplementary* Table S1) using Phusion High-Fidelity DNA Polymerase (New Englands Biolabs) and according to the following program: denaturation (98°C 10s), hybridization (69°C 30s) and amplification (72°C 1mn) during 38 cycles. Libraries were constructed with Ion Xpress Plus gDNA

Fragment Library kit (Cat. no. 4471269, Life Technologies) and sequenced on the Ion-Proton System S5. SHM frequencies were determined using Raw Data analyzed with DeMinEr tool [37]

RNA-Sequencing: RNA-Seq analysis was performed either on splenic resting B cells sorted with Easysep Mouse B cell isolation kit (Stem Cell Technologies), *in vitro*-activated B cells with LPS (bulk culture, at day 2) and *in vitro* LPS-differentiated plasmablasts (sorted at day 4). Sample quality controls and library preparation were performed at the GeT-Santé facility (Inserm, Toulouse, France, get.genotoul.fr). i/ Quality control: RNA concentration and purity were determined using a ND-2000 Spectrophotometer (Thermo Fisher Scientific, Waltham, USA). RNA integrity was checked with a Fragment Analyzer (Agilent Technologies, Santa Clara, USA), using the RNA Standard Sensitivity Kit. 260/280 purity ratios were all ≥ 1.8, and integrity indices were of good quality (8.3-10 RIN and > 1.7 28S/18S ratios). ii/ Library preparation (GeT-Santé): RNA-seq paired-end libraries were prepared according to Illumina's protocol with some adjustments, using the TruSeq Stranded Total RNA Gold library prep Kit (Illumina, San Diego, USA). Briefly, between 934-1000 ng total RNA were first ribo-zero depleted using Illumina Ribo-Zero probes. Then, remaining RNA were fragmented during 2 min and retrotranscribed to generate double stranded cDNA. Compatible adaptors were ligated, allowing the barcoding of the samples with unique dual indices. Libraries were amplified by 12 PCR cycles of PCR and an additional final purification step resulted in 280-700 bp fragments. Libraries quality was assessed using the HS NGS kit on the Fragment Analyzer (Agilent Technologies, Santa Clara, USA). iii/ Library quantification (GeT-PlaGe): quantification and sequencing were performed at the GeT-PlaGe core facility (INRAE, Toulouse, France). Libraries were quantified by qPCR using the KAPA Library Quantification Kit (Roche, Basel, Switzerland) to obtain an accurate quantification. iiii/ Sequencing (GeT-PlaGe): libraries were equimolarly pooled and RNA sequencing was then performed on one S4 lane of the Illumina NovaSeq 6000 instrument (Illumina, San Diego, USA), using the NovaSeq 6000 S4 v1.5 Reagent Kit (300 cycles), and a paired-end 2 x 150 pb strategy.

RNA-Sequencing Analysis: Paired-end reads were mapped on GRCm38 mouse genome that was previously indexed with "Mus_musculus.GRCm38.dna.primary_assembly.fa" and "Mus_musculus.GRCm38.102.chr_patch_hapl_scaff.gtf" files from ENSEMBL release 102. Index and mapping steps were both made with STAR v2.6.0c [44]. Then featureCounts v2.0.1 [45] was used to count reads by gene. An R script named template_script_DESeq2_CL.r of SARTools [46] was run first with all count data in order to retrieve a PCA and check if biological variability was the main source of variance in the data. Then, the same script was run for each desired differential analysis with count data from defined reference and interest conditions. Differentially regulated genes with an adjusted p value of 0.05 and a foldchange ≤ -1.5 or ≥ 1.5 were selected for downstream analysis. Gene SYMBOLs were converted to ENTREZIDs with the bitr function of the R ClusterProfiler

package [47]. The resulting ENTREZIDs and their associated log2foldchange were then used to calculate enriched biological pathway profiles of different gene clusters (Down in cKO , Up in cKO , Down in WT and Up in WT) using the CompareCluster function of ClusterProfiler [47] with p value and q value thresholds set to 0.01 and 0.05 respectively. The resulting enriched functional profiles were filtered through a Gene Ontology list consisting of the hierarchical children of the following Biological pathway terms: B cell costimulation, B cell selection, humoral immune response, immunoglobulin production, memory B cell differentiation, regulation of the apoptotic process of mature B cells, SHM (*Supplementary* Table S3). Terms that were enriched in all down-regulated gene clusters or all up-regulated clusters were discarded.

3C-HTGTS: 3C-HTGTS was performed as previously described[48]. Briefly, 10 million of resting and LPS-stimulated B cells (at day 3) were crosslinked with 2% formaldehyde 10% FCS PBS for 10min at RT under rotation. Crosslinking is stopped by adding glycine at 0.1M. Then, cells were lysed in 50mM Tris, 150mM NaCl, 5mM EDTA, 0.5%NP-40,1% TX-100 supplemented with protease inhibitor (ROCHE #11873580001). Nuclei were resuspended in 0,3% SDS for 1h at 37°C at 900rpm and then neutralized with Triton TX-100 for 1h. DNA restriction was performed using CviQ1 (Thermo Fisher ER0211) in B buffer (Thermo Fisher #BB5) overnight at 37 °C, before heat inactivation for 25 min at 65 °C. Overnight ligation was performed at 16°C at 300rpm. Next, DNA was treated by proteinase K and RNase and cleaned by phenol/chloroform. After 3C step, the LAM-HTGTS protocol was performed [49]. Briefly, 3C DNA was sonicated using the Bioruptor (Diagenode; two pulses at low intensity for 20s), and 10 µg was used for the LAM-HTGTS step. A Sµ bait was used for primer elongation. These single-stranded DNA fragments were incubated with streptavidin beads (Dynabeads C1 streptavidin beads; Invitrogen) overnight at RT and washed with BW buffer (1M NaCl, 5mM Tris-HCl pH7.4, 0,5mM EDTA pH 8.0). Universal I7 adaptors were ligated before the nested PCR performed with Sµ nested and universal I7 reverse primers (all primers are listed in *Supplementary* Table S1). After the Tagged PCR with I7 and I5 Illumina primer, PCR products were cleaned using PCR clean-up kit (Macherey-Nagel REF#740609) and validated after migration on BioAnalyser (Agilent). 3C-HTGTS libraries were sequenced 300pb paired-end MiSeq V3 with 20% PhiX.

Analysis of 3C-HTGTS: Sequencing reads were aligned to the mm10 genome and processed as previously described[49]. Each 3C-HTGTS library plotted for comparison was normalized by randomly selecting a number of junctions equal to the total number of junctions present in the smallest library in the comparison set.

Data availability: Raw data from RNA-seq, SHM, Rep-Seq and 3C-HTGTS have been deposited in the European Nucleotide Archive database under access number PRJEB52320.

Results

Conditional deletion of Satb1 in murine B lineage cells

Since depletion of *Satb1* in ES cells and mouse embryos showed multiple dysfunctions and did not allow animals to survive beyond 1 month of age [2], we evaluated SATB1 contribution to B cell development in a conditional knock out model inducing SATB1 depletion in B-lineage cells from the pro-B cell stage. In our model, initially derived from *Satb1*^{tm1a} allele, *Satb1* conditional allele (*Satb1*^{flx}) contains exon 4 flanked with two *LoxP* sites that permit its specific deletion when coupled to one allele carrying a CRE recombinase insertion into *Cd79a* gene (*Cd79a*^{cre}) [36] (Fig. 1*A*). Mice carrying the homozygous SATB1 deletion in B-lineage cells (*Satb1*$^{flx/flx}$ *Cd79a*$^{cre/+}$, referred as cKO conditional Knock Out) were compared to heterozygous littermates (*Satb1*$^{flx/+}$ *Cd79a*$^{cre/+}$, referred as cHet: conditional Heterozygous) and to *wt* littermates carrying an identical conditional allele but devoid of CRE expression (*Satb1*$^{flx/+}$ *Cd79a*$^{+/+}$, referred as WT). Western blot experiments performed on sorted splenic B cells from these three genotypes confirmed that *Satb1*-exon4 deletion induced a complete protein depletion (Fig. 1*B,* unprocessed raw data are provided in *Supplementary* Fig. S1).

SATB1 depletion in B lineage cells allows normal B cell development and IgH repertoire

By questioning ImmGen database [50], we examined *Satb1* expression in developing B-lineage cells and noted that all subtypes of B-lineage cells expressed *Satb1* transcripts (*Supplementary* Fig. S2*A*). Common lymphoid progenitor and pre-pro B cells, also mentioned as Hardy fraction A, both displayed higher SATB1 expression. This was not surprising given that SATB1 has been reported to favor lymphocyte lineage differentiation from hematopoietic stem cells [23]. While a consistent drop in *Satb1* transcription was observed at pro- and pre-B stages, a second wave of *Satb1* gene expression occured in transitional and mature resting B cells present in splenic follicles or the marginal zone as well as in splenic memory B cells. *Satb1* gene expression further decreased in antigen-activated cells such as germinal center centrocytes to reach its minimal level in proliferating cell subsets such as centroblasts and plasmablasts (*Supplementary* Fig. S2*A*). In B cells from WT mice, we experimentally confirmed a significant decrease in *Satb1* transcripts by RT-qPCR assays when comparing naive and GC B cells sorted from Peyer's patches (Fig. 1*C*). The same findings, corroborating expression profiles described in the ImmGen database, were very recently documented in a mouse model carrying a Tomato-reporter transgene knocked into a *Satb1* allele [35]. This converging evidence for variable expression of *Satb1,* according to B cell subsets, supposes a narrow regulation and suggests an accurate function of this factor in the B cell lineage.

To determine SATB1 contribution throughout B cell development and maturation, we analyzed B cell populations from WT, cHet and cKO mice by flow cytometry (*Supplementary* Fig. S1). Absolute numbers of B-lineage cell subsets from bone marrow (Fig. 1*D* left and middle) and spleen (Fig. 1*D* right) were not affected by *Satb1* gene inactivation suggesting, despite its contribution to lymphocyte lineage initiation [22], that SATB1 was not required for B cell development. Our findings that early B cell development was not impaired in our cKO mice excluded any function for SATB1 in B-lineage choice maintenance. This data completed studies from Kanakura and Steidl groups [21,22] that previously hypothesized that SATB1 function was restricted to stem cell renewal and fate hematopoietic lineages.

Since SATB1-binding to the ASE region is known to modulate *Rag* gene expression in T cells and incidentally impact TCR rearrangements [33], the consistent expression of this factor in early committed and developing B cells could confer a similar function on Ig gene rearrangements. We investigated this point by first analyzing *Rag* gene expression by RT-qPCR and found that sorted bone marrow pre-B cells from WT and cKO animals expressed similar transcript levels (*Supplementary* Fig. S2*B*). The striking different impact of SATB1 deletion on *Rag* expression in B and T cells could be indirectly explored by comparing DNA accessibility in the region close to *Rag* genes regions from WT B- and T-lineage cell precursors. Such a detailed study was provided by the consortium of the Immunological Genome Project that performed ATAC-seq in B and T cell precursors[51]. This study indicates that, while the DNA region encompassing the SATB1-binding ASE regulatory element was accessible in T-lineage precursor cells, this was not the case in bone marrow cell subsets of the B cell lineage (a comparison focused on *Rag* gene loci was provided in *Supplementary* Fig. S2*C*). To note, B-lineage precursors display other accessible regulatory regions such as the *Erag* element located closely to Rag genes regions. It is then reasonable to suppose that ASE region is not active in the B cell lineage, this could potentially explain normal *Rag* gene transcription in SATB1-deficient B cell precursors. Given that SATB1 acts as a chromatin loop organizer in T cells [5,34,52–54], we suspected a potential effect of its deletion on *IgH* V region accessibility in developing B cells. To assess this point we examined VDJ recombination diversity by Repertoire-Sequencing experiments on RNA samples (RepSeq) extracted from pre-B cell-enriched bone marrow fractions. Our data displayed an equivalent broad distribution of each rearranged and expressed V gene (Fig. 1*E* and *Supplementary* Fig. S2*D*) in WT and cKO mice. A similar representation of V_H family usage indicated that SATB1 deletion did not hamper mechanisms leading to a diversified *IgH* VDJ repertoire in developing B cells. VDJ junction analysis in pre-immune repertoire of WT and *Satb1* cKO models revealed comparable lengths of CDR3 regions as well as rather comparable distribution of P and N nucleotides (*Supplementary* Fig. S2*E*) suggesting that *IgH V* region assembly and end-joining occurs normally in the absence of STAB1. Altogether, our results indicate that SATB1 is dispensable to establish *IgH* repertoire and does not

affect *Rag* expression or influence *IgH* locus accessibility. Given that SATB1 deletion did not impair VDJ rearrangements and B cell development, further studies could then be performed on peripheral B cell subsets in this model without any bias. In line with this statement, we determined whether SATB1 deletion could impact Ig isotype production and secretion in the mouse. Sera from WT, cHet and cKO animals were collected at two months of age and IgM, IgG1, IgG3 and IgA levels were quantified by ELISA assays. Homozygous and heterozygous KO mice displayed serum Ig levels comparable to WT for each isotype (Fig. 1*F*), suggesting that SATB1 does not influence global antibody production.

SATB1 depletion decreases IgH transcription in resting B cells

Despite normal bone-marrow B cell development and Ig secretion in cKO mice, we however suspected that SATB1 depletion might influence *IgH* locus expression, given its capacity to bind MAR sequences *in vitro* [55] and to modulate MAR-containing reporter genes [29]. We first examined surface IgM expression levels, as a component of B cell receptors, on immature and mature B cell subsets from bone marrow and spleen compartments in our model. By measuring IgM mean fluorescence intensity (MFI) by flow cytometry, *Satb1* cKO mice displayed consistent and significant decreased IgM surface expression when compared to WT, on bone marrow immature and recirculating B cells (Fig. 2*A*) and on splenic transitional, marginal zone and follicular B cell populations (Fig. 2*B*). The same significant decrease in IgM BCR expression, also observed on naive B cells sorted from Peyer's patches (Fig. 2*C*), confirmed a specific function for SATB1 as a positive regulator of BCR expression in resting B cells. This role for SATB1 in BCR surface expression could explain its function as a contributing factor to B cell survival as described recently by Ozawa et al [35]. Indeed, the knock-in reporter mouse model used in their study leads to inactivation of one *Satb1* allele and it is likely that such a deletion induces intermediate surface IgM expression level similar to the one we observed in our heterozygous mice (*Supplementary* Fig. S3 A). It is reasonable to suppose that reduced BCR expression on resting B cells reduces ability of these cells to respond to anti-IgM mediated *in vitro*-stimulation. One fair interpretation of the survival defect described by Ozawa et al [35] could be simply the consequence of reduced BCR expression in the knock-in model.

The decreased BCR expression observed in SATB1-deficient B lymphocytes raised the question of a potential Ig gene transcription defect in our model. Quantification of *IgH* primary transcription by RT-qPCR in resting splenic B cells showed a significant 2 fold-decrease of transcripts running through the J_H4 intron in cKO mice when compared to WT (Fig. 2*D*). We also evaluated the respective proportion of membrane and secreted *Igμ* transcripts (*Supplementary* Fig. S3*B*), our data showed that SATB1 deletion does not impair alternative splicing of the *Igμ* chain transcript. Although not statistically significant, a similar downward trend was also observed for *Igκ*

transcription in mutants (Fig. 2*D*). It is established that MAR sequences flanking both sides of the *IgH cEμ* intronic enhancer are able to bind SATB1 [56]. Whereas binding of equivalent regions in the *Igκ* locus has never been shown, it has to be noted that only one upstream MAR is associated with the *iEκ* enhancer. The presence of either one or two MAR sequences surrounding these intronic enhancers could potentially explain differences observed for *IgH* and *Igκ* transcription in our *Satb*1 KO model. It is tempting to speculate that, through its DNA binding in proximity to intronic enhancers, SATB1 could physiologically potentiate their transcriptional effect in resting B cells. Although, this hypothesis is unlikely since IgM BCR expression was never compromised in resting B cell populations of mice devoid of either *Eμ*, *iEκ* full regions or their associated-MARs [57–60]. In contrast, the literature reports that BCR expression on resting B cells was decreased upon deletion of components of the 3'regulatory regions of both *IgH* [61] and *Igκ* [62] loci, arguing for the importance of close contact between 3'enhancers and respective promoters of rearranged V exons. In resting B cells, such loops have been reported within the *IgH* locus in many studies [63]. In line with a proposed function for SATB1 as a promoter-enhancer loop regulator[54], a rationale hypothesis could be that this MAR binding protein participates in physical interactions between rearranged V_H exons and the *3'RR* and consequently enhances Ig chain transcription in resting B cells. To evaluate such chromatin loop interactions, we performed 3C-HTGTS experiments using a bait within the *Sμ* region[48] of resting B cells from *wt* and mutant mice. Our data showed that loop interactions between *Eμ* and V_H regions still occur at frequencies that do not significantly differ in resting B cells from both genotypes (*Supplementary* Fig. S4*A*); this suggests that SATB1 is not required to form chromatin loops in naive and LPS-activated B cells.

In line with the broad chromatin organization function proposed for SATB1 in T cells, we then performed total RNA seq analysis of both WT and SATB1-deficient B cell subsets. Resulting datasets were submitted to principal component analysis to validate reproducibility between samples (*Supplementary* Fig. S5*A*). When comparing datasets obtained from resting splenic B cells, our analysis only disclosed 65 genes displaying significant changes in expression: 53 were overexpressed and only 12 were downregulated (log2 FC>+/-1.5; Fig. 2*E* and *Supplementary* Table S4). Indeed, our data supports the hypothesis of an ambivalent function for SATB1, displaying both positive and negative regulatory actions for gene expression in resting B cells. Our study indicates that SATB1 depletion does not induce drastic transcriptional changes in resting B cells. In contrast to the T lineage [7,27,64], our data suggest that the intrinsic function of SATB1 in B cells may be relatively focused. In this cell type, SATB1 would have a distinctly different role from that of a major genome organizer.

SATB1 depletion increases IgH transcription and Ig synthesis in activated B cells

We sought to evaluate effect of SATB1 depletion on B cell activation in response to mitogenic and antigenic stimuli. We first performed *in vitro* stimulation of splenic B cells from both genotypes with LPS and carried out RNA seq in a time-course manner on resting B cells (sorted at day 0), activated B cells (bulk culture at day 2) and plasmablasts (sorted at day 4). Once sample reproducibility validated (*Supplementary* Fig. S5*A*), we compared transcriptional programs induced by transition from "resting to activated" and "activated to plasmablast" cell stages. Venn diagrams mainly indicate that both B cell activation and differentiation programs induced by LPS were not drastically impaired upon SATB1 depletion. Indeed, following *in vitro* culture, a vast majority of transcripts displayed a common regulation profile in WT and SATB1-deficient models: *i.e.* 5460 transcripts during the "resting to activated" transition and 2758 during the "activated to plasmablast" transition (*Supplementary* Fig. S5*B*). Nevertheless, we submitted differentially expressed genes from both transition programs, to a gene ontology analysis for biological processes relevant to B cell activation (see list in *Supplementary* Table S3). During the "resting to activated" transition, SATB1 depletion decreased expression of a few genes involved in humoral immune responses mediated by circulating immunoglobulins (Fig. 3*A,* red dots) including *Lta,* a gene recently described as a SATB1 target in T cells [54], as well as *Tgfb1* encoding TGFβ, the cytokine involved in regulation of isotype switching to IgA. Strikingly, the analysis specified that SATB1 depletion increased *Tcf3* expression in activated B cells (Fig. 3*A,* blue dot), while its gene expression, encoding the E2A transcription factor, was unchanged in hematopoietic stem cells devoid of SATB1 [65]. During the "activated to plasmablast" transition, SATB1 depletion downregulates *Cd40* and few genes involved in Ig class switching pathway (Fig. 3*B,* red dots); this effect on *Cd40* targeting was expected since already observed upon SATB1 deletion in hematopoietic stem cells and T cells [54,65].

In parallel, in such *in vitro* stimulation assays, B cells were tested for intrinsic abilities to proliferate, to undergo LPS-driven class switch recombination and to differentiate into plasmablasts. When measured by EDU incorporation, the ability of SATB1-deficient B cells to proliferate was similar to that of WT cells (*Supplementary* Fig. S6*A*). This suggested that, while decreasing IgM BCR expression on naive cells, SATB1-deficiency is dispensable for cell cycle entry of splenic B cells upon activation of TLR pathways. The same normal proliferation capacity in response to TLR or CD40 triggering was also recently reported for B cells devoid of the entire *Satb1* gene region [35]. In our model, normal *in vitro* proliferation observed in B cells devoid of SATB1 was consistent to the normal proportion of spontaneous GC B cells in Peyer's patches of KO animals (Fig. 3*C*), or the equivalent proportions of splenic GC centroblasts and centrocytes obtained after NP-CGG immunization (*Supplementary* Fig. S6*B*). More strikingly, in clear contrast with the decreased *IgH* expression in resting B cells, such *in viv*o-activated cells express higher BCR levels as evidenced by IgM surface labelling (Fig. 3*D*). This highlights that the ambivalent function for SATB1 clearly applies to Ig gene expression in developing mature B cells.

Class switching to IgG3 was examined by surface labelling of *in vitro*-activated splenic B cells by LPS at day 4. Data showed equivalent numbers of IgG3-expressing cells in both WT and SATB1 KO models (*Supplementary* Fig. S6*C*) indicating that SATB1 is not required for IgG3 class switching. RNA seq datasets from LPS- activated cells at day 2 also provided relevant portrayals of germline transcription landscape in the *IgH* locus of WT and SATB1 deficient models (*Supplementary* Fig. S6*D*). When examining germline transcription within the *Iμ*-donor and *Iγ3*- or *Iγ2b*-acceptor regions, both WT and SATB1-deficient models displayed identical profiles suggesting that, in agreement with normal CSR to IgG3 observed at day 4, SATB1 depletion does not impede LPS-induced germline transcription occurring prior to CSR.

When measured in the same *in vitro* assays, the intrinsic ability of splenic B cells to differentiate into plasmablasts ($CD138^+$) upon LPS activation was also similar in WT and our SATB1 KO model (Fig. 3*E*). In agreement with *in vitro* data, NP-CGG immunization of mice induced generation of plasma cells in normal proportions in the absence of SATB1 (Fig. 3*F*). Altogether, these data suggest that SATB1 is dispensable for efficient differentiation into antibody secreting cells.

Although, once differentiated *in vitro* into plasmablasts, SATB1 deficient cells displayed higher levels of intracellular IgM when analyzed by flow cytometry (Fig. 3*G*). This increase in Ig production by plasmablasts was correlated with a significant increase of both *IgH* and *Igκ* primary transcripts (respectively 1.4 and 1.7) in LPS-activated cells from SATB1 deficient animals (Fig. 3*H*).

The effect of SATB1 deletion on global transcription of both IgH and IgL chains was also confirmed by comparing RNA seq data from splenic B cells activated by LPS at day 2 (Fig.3*J*) or from sorted plasmablasts at day 4 (Fig.3*K*). In the first case, among the 64 genes found upregulated in SATB1-deficient models (log2 FC>+/-1.5), 20 of them corresponded to *IgV* H chain products and 23 others were identified as *IgV* κL chain products (Fig.3*J* and *Supplementary* Table S5). When comparing plasmablasts, *IgV* H chain and *IgV* λL chain products were strongly increased upon SATB1 depletion (Fig. 3*K* and *Supplementary* Table S6). Our data indicate that, beyond its modest effect on B cell activation programs induced by LPS *in vitro*, the absence of SATB1 induces a more pronounced transcription of Ig genes. Moreover, STAB1 is dispensable for proliferation, CSR and differentiation into plasma cells.

As a parallel to LPS stimulation, we performed *in vitro* stimulation with anti-CD40+IL4 in our model to evaluate, in another activation context, cell differentiation and Ig intracellular content in the absence of SATB1. Our data show, as in LPS-stimulation, that SATB1-deficient B cells differentiate efficiently into plamablasts in response to anti-CD40+IL4 cocktail (Supplementary Fig S6*E left*). To note, such plasmablasts devoid of SATB1 also contains high level of intracellular IgM, although upregulation was not, in this case, increased significantly (Supplementary Fig S6*E right*). However, our data unveil a switch in the regulatory function of SATB1 for Ig chain transcription, from positive in naive to negative in activated B cells. This striking effect persists until the terminal stage since

SATB1-deficient plasma cells display a high content of Ig chains. However, SATB1-depletion does not allow plasma cells to produce more Ig since our deficient mice display broadly normal levels of serum antibody isotypes.

SATB1 depletion increases somatic hypermutation

Since our group recently reported a critical function of *cEμ*-associated MARs for SHM of the *IgH* locus in mouse models [66], and according to historic studies in the *Igκ* locus [59], it was questionable whether MAR binding proteins, such as SATB1, could be involved in targeting somatic mutations of Ig genes. We first evaluated the ability of SATB1 deficient B cells to support somatic mutations by analyzing global SHM within intronic regions, not subject to antigen selection, located immediately downstream from V exons of both *IgH* and *Igκ* loci and also upstream from *IgH Sμ* regions in spontaneous GC B cells from Peyer's patches. As a possible regulation mechanism, transcription taking place in the corresponding regions targeted by AID was also quantified in this subset. Second, to more accurately evaluate the ability of SATB1-deficient B cells to undergo SHM in response to specific antigen, we immunized mice with NP-CGG [67]. By analogy to B cells devoid of $MARs_{E\mu}$ regions, in which SHM machinery gains access more frequently to the region downstream from *cEμ* (upstream from *Sμ*) [68], we carefully quantified SHM in this same region (Fig 4*A, scheme*). In GC B cells sorted from Peyer's patches, while *Sμ* transcription was not significantly raised (Fig. 4*A, left bar graph*, p=0.3), we found a significant increase of mutations in the absence of SATB1 (1.88 mut/Kb) compared to WT (1.44 mut/Kb) (Fig. 4*A, middle bar graph*, p=0.02 and *Supplementary* Table S7*A*). A similar and significant increase of SHM in this region was also observed in splenic GC B cells sorted after NP-CGG immunization: while WT cells barely reached 0.22 mut/Kb, SATB1-deficient cells underwent two fold more mutations reaching 0.41 mut/Kb (Fig. 4*A, right bar graph*, p=0.03 and *Supplementary* Table S7*B*). This common feature shared by $MARs_{E\mu}$ KO- and *Satb1* KO-B cells suggests that SATB1 could be involved in limiting access of the SHM machinery to donor *Sμ* regions in cells undergoing SHM. When transcription and SHM were quantified downstream from the rearranged *IgH* variable regions (Fig 4*B*, scheme) in GC B cells sorted from Peyer's patches, homozygous *Satb1* deletion increased transcription (Fig. 4*A, left bar graph*, p=0.3) downstream from J_H4 and raised, although not significantly, SHM frequencies (Fig. 4*B, middle bar graph*, p=0.05 and *Supplementary* Table S7*C*). These findings were clearly confirmed upon NP-CGG immunization. Since B cell response to NP-CGG challenge is preferentially dominated by mutated clones expressing the V_H186.2 segment [67], quantification of base substitutions in the J_H4 intron downstream from the V_H186.2-rearranged exons is considered as a reliable hallmark of antigen-induced SHM. Indeed, in SATB1-deficient GC B cells from immunized mice, NP-CGG-induced mutations were significantly increased within the J_H4 intron: mutant cells displayed 5.06 mut/Kb while WT cells only reached 3.28 mut/Kb (Fig. 4*B, right bar*

graph, p=0.02 and *Supplementary* Table S7*D*). When, in the intronic region downstream from *Jκ5* of the *Igκ* locus (Fig 4*C,* scheme), global transcription was significantly increased in mutant samples, (Fig 4*C, left bar graph*, p=0.03), both spontaneous and NP-CGG-induced GC B cells displayed an increased trend of mutation frequencies upon SATB1 depletion (Fig. 4*C, middle and right bar graphs* and *Supplementary* Table S7*E and F*). Since B cell responses to DNP hapten preferentially involve Ig composed of Igλ1 light chains [69], it is likely that changes in mutation frequency within the *Igκ* light chain loci, in this case not significant, probably underestimated any potential SHM increase induced by SATB1 depletion. While our Gene Ontology enrichment analysis detects the "Somatic diversification of Igs" as a differentially regulated pathway during the "resting to activated" transition, expression of major actors of mismatch repair (MMR) and base excision repair (BER) pathways such as *Ung, Msh2, Msh6, Pms2* and *Polq* were similarly upregulated in both wt and cKO samples (Fig. 3*A*). Beyond global pathways analysis, it was also necessary to verify in detail whether SATB1 depletion could affect, through its transcription factor function, expression of any potential factors, including AID, involved in SHM. Indeed, when extracted from RNA-seq datasets, expression of 16 genes involved in SHM was unchanged upon SATB1 deletion in both LPS-activated B cells as well as LPS-induced plasmablasts (*Supplementary* Fig. S7*A*). Within Ig gene regions submitted to SHM analysis, substitution frequencies calculated at each base displayed a globally increased pattern (although not significant) that did not offer any hypothesis regarding the origin of the changes (*Supplementary* Fig. S7*B*). It is well established that AID targeting for SHM is coupled to transcription initiated at V promoters [70]. Given the significant increase of primary transcription occurring at *IgH* and *Igκ* in GC B cells devoid of SATB1 (Fig. 4*B* and 4*C*), one straightforward hypothesis to explain the global SHM increase in our model could be an overall increase in AID targeting of Ig genes. Interestingly, in line with this hypothesis, we recently highlighted increased AID deamination coupled to increased transcription in our mouse model devoid of $MARs_{E\mu}$ regions when bred into a DNA repair-deficient background [68]. Surprisingly, while genomic deletion of MAR_{Eik} or $MARs_{E\mu}$ regions in the mouse decreased SHM [59,68], suppression of SATB1 led to the opposite effect in the regions downstream from the rearranged variable segments of *IgH* and *Igκ* loci. This finding also plays in favor of a protective function for SATB1 against mutations. In this case, since the regions involved are located upstream from *Eμ* and *Eiκ*, one could propose that the potential protective effect of SATB1 could take place in resting B cells in which SHM is not expected to happen. Moreover, the discrepancy between the effect of $MARs_{E\mu}$ deletion and SATB1-depletion on targeted mutations upstream from intronic enhancers suggest that other interacting factors, beyond SATB1, participate in the complex regulation of *cis*-acting MARs. While we recently proposed that $MARs_{E\mu}$ favor error-prone repair in its upstream regions in order to optimize SHM [68], our current study suggest that SATB1 does not participate in the unfaithful repair processes associated with SHM.

Taken together, our data suggest that SATB1-deletion increases SHM of Ig genes through a transcription-coupled mechanism that probably favors AID targeting.

Discussion

The fact that SATB1 plays a major role as a "genome organizer" in hematopoietic- and T-lineage cells [7,28,30] suggested that it is also important in B-lineage cells, a cell type that also undergoes fine developmental regulation of its expression [35]. By using a conditional deletion model in B cells, our study fills in gaps concerning the function of SATB1 in this lymphocyte lineage. In contrast to its function in early-developing T cells, SATB1 is dispensable for the establishment of the Ig gene repertoire and overall early B cell development in the bone marrow; this result is consistent with the pioneer SATB1-null mouse model in which B cell populations could be observed in the spleen[2]. When looking at regions involved in *Rag* genes regulation, accessibility data suggests that, unlike its critical function in T cell precursors, ASE region is not active in B-lineage cells. This difference suggests that *Rag* genes regulation process evolved separately in B and T lineages, at least with regard to the regulatory function of SATB1. However, our model reveals that SATB1 is involved in the control of Ig gene transcription in mature B cells. Although previously unknown in the B lineage, our findings once again point to a dual function for SATB1 depending on the activation stage. We show that SATB1 promotes Ig gene transcription in resting B cells, while in activated B cells, it acts as a repressor. In contrast to the T cell lineage where SATB1 is considered a major regulatory factor of the enhancer/super-enhancer network [53,54], SATB1 deletion does not induce major disruptions in the B cell transcriptome. Our invalidation model shows that only a reduced number of genes expressed during B differentiation are impacted by SATB1 deletion. In agreement with the repressive function of this factor in activated B cells, our study also shows that Ig genes are the predominant targets of SATB1 in activated B cells. Our 3C-HTGTS data indicate that SATB1 is not required to establish chromatin loops between *Eμ* and V_H regions in resting and activated B cells. A rationale hypothesis could be that the effect of SATB1 on *IgH* transcription is mainly due to its function as a transcription factor rather than a genome organizer. Given the critical effect of SATB1 depletion on Ig gene transcription, it would certainly be interesting to evaluate SATB1 physiological binding to regulatory regions in Ig gene loci in resting and activated B cells.

By clarifying that SATB1 is an essential activator of Ig chain transcription, and consequently BCR expression, in resting B cells, our study extends recent work published by Yokota's team [35] and proposes a rational explanation for the survival function of SATB1 at this stage. These two studies also point out the importance of SATB1 expression levels which could, as demonstrated in HSCs [22,65], fine-tune some critical genes or regulatory pathways in lymphocytes. Beyond the physiological decrease in *Satb1* expression between naive and activated B stages, it is possible that this gene

undergoes splicing modifications in the B cell lineage as it is proposed in developing T cells by the Spillianakis' group [71]. The stability of SATB1 protein, according to its transcript variants, might also be critical for its function in mature B cell subsets, as already proposed in T-lineage cells by the Galande's group[19]. Interestingly, the dual function of SATB1 also observed in the B lineage, switching from activator to repressor of transcription in activated B cells, is reminiscent of the molecular switch observed upon phosphorylation and acetylation of this factor [16].

A surprising observation from our study is that SATB1 deletion increases somatic hypermutation of the *IgH* locus, extending into the *Sμ* region. It is very likely that the *Igκ* locus is similarly influenced. A direct impact of SATB1 on key factors involved in SHM, such as AID and proteins involved in BER and MMR pathways, can be excluded since normal induction of their transcripts were observed in the absence of SATB1. In this respect, SATB1 could play a protective role against SHM in resting cells. This finding should be read in conjunction with our recent study of the MARs regions associated with the *Eμ* enhancer of the *IgH* locus [68], known to bind SATB1 [1]. The SATB1-induced increase in SHM could logically be correlated with the observed increase in primary transcription of the variable regions of Ig H and L chains. However, it is not excluded that SATB1 modifies the accessibility of these regions to AID or its cofactors. Since it is proposed that SATB1 stabilizes the unpaired DNA regions against unwinding [13], such an action of SATB1 taking place in the *MARs-Eμ* region could contribute to the protection of its surrounding regions against unwanted SHM. In line with the putative protective function of SATB1, it has been shown that this protein acts as an accessory factor of BER through its interaction with Oxo-guanine-glycosylase 1 (OGG1) [72], a DNA glycosylase that usually promotes error-free repair and that is not involved in Ig gene SHM [73].

Further study of these modifications of SATB1 in B cells will be necessary to clarify the origin of its versatility. It has recently been proposed that SATB1 isoforms are subject to phase separation in T cells [71]. Consistent with its localization to PML nuclear bodies [74,75], this mode of regulation deserves to be explored in the context of the B cell nucleus. Moreover, since chromatin loop extrusion mechanisms are now proven to be critical for Ig gene regulation [76], it might be relevant to evaluate a potential implication of SATB1 in this process.

Acknowledgments

The authors are grateful to BISCEm unit (Univ. Limoges, UAR 2015 CNRS, US 42 Inserm, CHU Limoges) for technical support regarding DNA-RNA sequencing, cytometry experiments and animal core facility. We are grateful to Emeline Lhuillier and the Genotoul Plateau GeT-Santé facility (https://get.genotoul.fr) for technical assistance with RNA sequencing, to Mehdi Alizadeh from Etablissement Français du Sang (Rennes; France) for assistance with Repertoire sequencing and to Christelle Oblet for technical help with Western blots. This work benefitted from data

assembled by the ImmGen consortium[50]. MT, CB and OM were supported by PhD fellowships from the French Ministère de l'Enseignement Supérieur, de la Recherche et de l'Innovation and the Fonds Européen de Développement Régional (FEDER). This work was supported by La Ligue Contre le Cancer (comités 87, 23 to EP and SLN); the Fondation ARC pour la recherche sur le cancer (PJA 20181207918 to EP and PhD continuation fellowship to MT and CB), Institut CARNOT CALYM, INCa-Cancéropôle GSO Emergence (to EP). We are grateful to Drs. Jeanne Moreau and Amélie Bonaud for critical reading of the manuscript, helpful comments and edits.

Author Contributions: MT, CB, OM, SB and CC performed experiments. MT analyzed the data. EP and SLN conceived and supervised the study. MT and OM developed the experimental model. JP performed the bio-informatic analysis. MT, CB, EP and SLN wrote the manuscript.

Competing Interest Statement: The authors declare no competing financial interests.

References

1 Dickinson L, Tadashi J, Yoshinori K, Terumi K-S. A tissue-specific MARSAR DNA-binding protein with unusual binding site recognition. *Cell* 1992; **70**: 631–645.

2 Alvarez JD, Yasui DH, Niida H, Joh T, Loh DY, Kohwi-Shigematsu T. The MAR-binding protein SATB1 orchestrates temporal and spatial expression of multiple genes during T-cell development. *Genes Dev* 2000; **14**: 521–535.

3 Cai S, Han H-J, Kohwi-Shigematsu T. Tissue-specific nuclear architecture and gene expession regulated by SATB1. *Nat Genet* 2003; **34**: 42–51.

4 Yasui D, Miyano M, Cai S, Varga-Weisz P, Kohwi-Shigematsu T. SATB1 targets chromatin remodelling to regulate genes over long distances. *Nature* 2002; **419**: 641–645.

5 Cai S, Lee CC, Kohwi-Shigematsu T. SATB1 packages densely looped, transcriptionally active chromatin for coordinated expression of cytokine genes. *Nat Genet* 2006; **38**: 1278–1288.

6 Kohwi-Shigematsu T, Poterlowicz K, Ordinario E, Han H-J, Botchkarev VA, Kohwi Y. Genome organizing function of SATB1 in tumor progression. *Semin Cancer Biol* 2013; **23**: 72–79.

7 Zelenka T, Spilianakis C. SATB1-mediated chromatin landscape in T cells. *Nucl Austin Tex* 2020; **11**: 117–131.

8 Wang Z, Yang X, Chu X, Zhang J, Zhou H, Shen Y *et al.* The structural basis for the oligomerization of the N-terminal domain of SATB1. *Nucleic Acids Res* 2012; **40**: 4193–4202.

9 Purbey PK, Singh S, Kumar PP, Mehta S, Ganesh KN, Mitra D *et al.* PDZ domain-mediated dimerization and homeodomain-directed specificity are required for high-affinity DNA binding by SATB1. *Nucleic Acids Res* 2008; **36**: 2107–2122.

10 Yamasaki K, Akiba T, Yamasaki T, Harata K. Structural basis for recognition of the matrix attachment region of DNA by transcription factor SATB1. *Nucleic Acids Res* 2007; **35**: 5073–5084.

11 De Belle I, Cai S, Kohwi-Shigematsu T. The Genomic Sequences Bound to Special AT-rich Sequence-binding Protein 1 (SATB1) In Vivo in Jurkat T Cells Are Tightly Associated with the Nuclear Matrix at the Bases of the Chromatin Loops. *J Cell Biol* 1998; **141**: 335–348.

12 Seo J, Lozano MM, Dudley JP. Nuclear Matrix Binding Regulates SATB1-mediated Transcriptional Repression. *J Biol Chem* 2005; **280**: 24600–24609.

13 Ghosh RP, Shi Q, Yang L, Reddick MP, Nikitina T, Zhurkin VB *et al.* Satb1 integrates DNA binding site geometry and torsional stress to differentially target nucleosome-dense regions. *Nat Commun* 2019; **10**. doi:10.1038/s41467-019-11118-8.

14 Kumar PP, Purbey PK, Ravi DS, Mitra D, Galande S. Displacement of SATB1-Bound Histone Deacetylase 1 Corepressor by the Human Immunodeficiency Virus Type 1 Transactivator Induces Expression of Interleukin-2 and Its Receptor in T Cells. *Mol Cell Biol* 2005; **25**: 1620–1633.

15 Galande S, Purbey PK, Notani D, Kumar PP. The third dimension of gene regulation: organization of dynamic chromatin loopscape by SATB1. *Curr Opin Genet Dev* 2007; **17**: 408–414.

16 Pavan Kumar P, Purbey PK, Sinha CK, Notani D, Limaye A, Jayani RS *et al.* Phosphorylation of SATB1, a global gene regulator, acts as a molecular switch regulating its transcriptional activity in vivo. *Mol Cell* 2006; **22**: 231–243.

17 Purbey PK, Singh S, Notani D, Kumar PP, Limaye AS, Galande S. Acetylation-dependent interaction of SATB1 and CtBP1 mediates transcriptional repression by SATB1. *Mol Cell Biol* 2009; **29**: 1321–1337.

18 Khare SP, Shetty A, Biradar R, Patta I, Chen ZJ, Sathe AV *et al.* NF-κB Signaling and IL-4 Signaling Regulate SATB1 Expression via Alternative Promoter Usage During Th2 Differentiation. *Front Immunol* 2019; **10**: 667.

19 Patta I, Madhok A, Khare S, Gottimukkala KP, Verma A, Giri S *et al.* Dynamic regulation of chromatin organizer SATB1 via TCR-induced alternative promoter switch during T-cell development. *Nucleic Acids Res* 2020; **48**: 5873–5890.

20 Balamotis MA, Tamberg N, Woo YJ, Li J, Davy B, Kohwi-Shigematsu T *et al.* Satb1 Ablation Alters Temporal Expression of Immediate Early Genes and Reduces Dendritic Spine Density during Postnatal Brain Development. *Mol Cell Biol* 2012; **32**: 333–347.

21 Will B, Vogler TO, Bartholdy B, Garrett-Bakelman F, Mayer J, Barreyro L *et al.* Satb1 regulates the self-renewal of hematopoietic stem cells by promoting quiescence and repressing differentiation commitment. *Nat Immunol* 2013; **14**: 437–445.

22 Doi Y, Yokota T, Satoh Y, Okuzaki D, Tokunaga M, Ishibashi T *et al.* Variable SATB1 Levels Regulate Hematopoietic Stem Cell Heterogeneity with Distinct Lineage Fate. *Cell Rep* 2018; **23**: 3223–3235.

23 Satoh Y, Yokota T, Sudo T, Kondo M, Lai A, Kincade PW *et al.* The Satb1 Protein Directs Hematopoietic Stem Cell Differentiation toward Lymphoid Lineages. *Immunity* 2013; **38**: 1105–1115.

24 Wen J, Huang S, Rogers H, Dickinson LA, Kohwi-Shigematsu T, Noguchi CT. SATB1 family protein expressed during early erythroid differentiation modifies globin gene expression. *Blood* 2005; **105**: 3330–3339.

25 Hawkins SM, Kohwi-Shigematsu T, Skalnik DG. The Matrix Attachment Region-binding Protein SATB1 Interacts with Multiple Elements within the gp91 ^{phox} Promoter and Is Down-regulated during Myeloid Differentiation. *J Biol Chem* 2001; **276**: 44472–44480.

26 Fujii Y, Kumatori A, Nakamura M. SATB1 Makes a Complex with p300 and Represses gp91phox Promoter Activity. *Microbiol Immunol* 2003; **47**: 803–811.

27 Naik R, Galande S. SATB family chromatin organizers as master regulators of tumor progression. *Oncogene* 2019; **38**: 1989–2004.

28 Papadogkonas G, Papamatheakis D-A, Spilianakis C. 3D Genome Organization as an Epigenetic Determinant of Transcription Regulation in T Cells. *Front Immunol* 2022; **13**: 921375.

29 Kohwi-Shigematsu T, Maass K, Bode J. A thymocyte factor SATB1 suppresses transcription of stably integrated matrix-attachment region-linked reporter genes. *Biochemistry* 1997; **36**: 12005–12010.

30 Burute M, Gottimukkala K, Galande S. Chromatin organizer SATB1 is an important determinant of T-cell differentiation. *Immunol Cell Biol* 2012; **90**: 852–859.

31 Kakugawa K, Kojo S, Tanaka H, Seo W, Endo TA, Kitagawa Y *et al.* Essential Roles of SATB1 in Specifying T Lymphocyte Subsets. *Cell Rep* 2017; **19**: 1176–1188.

32 Kitagawa Y, Ohkura N, Kidani Y, Vandenbon A, Hirota K, Kawakami R *et al.* Guidance of regulatory T cell development by Satb1-dependent super-enhancer establishment. *Nat Immunol* 2017; **18**: 173–183.

33 Hao B, Naik AK, Watanabe A, Tanaka H, Chen L, Richards HW *et al.* An anti-silencer– and SATB1-dependent chromatin hub regulates Rag1 and Rag2 gene expression during thymocyte development. *J Exp Med* 2015; **212**: 809–824.

34 Feng D, Li Z, Qin L, Hao B. The role of chromatin organizer Satb1 in shaping TCR repertoire in adult thymus. *Genome* 2021; **64**: 821–832.

35 Ozawa T, Fujii K, Sudo T, Doi Y, Nakai R, Shingai Y *et al.* Special AT-Rich Sequence-Binding Protein 1 Supports Survival and Maturation of Naive B Cells Stimulated by B Cell Receptors. *J Immunol* 2022; **208**: 1937–1946.

36 Hobeika E, Thiemann S, Storch B, Jumaa H, Nielsen PJ, Pelanda R *et al.* Testing gene function early in the B cell lineage in mb1-cre mice. *Proc Natl Acad Sci U S A* 2006; **103**: 13789–13794.

37 Martin OA, Garot A, Le Noir S, Aldigier J-C, Cogné M, Pinaud E *et al.* Detecting Rare AID-Induced Mutations in B-Lineage Oncogenes from High-Throughput Sequencing Data Using the Detection of Minor Variants by Error Correction Method. *J Immunol* 2018; **201**: 950–956.

38 Tinguely A, Chemin G, Péron S, Sirac C, Reynaud S, Cogné M *et al.* Cross talk between immunoglobulin heavy-chain transcription and RNA surveillance during B cell development. *Mol Cell Biol* 2012; **32**: 107–117.

39 Pascal V, Dupont M, de Rouault P, Rizzo D, Rossille D, Jeannet R *et al.* Demultiplexing Ig repertoires by parallel mRNA/DNA sequencing shows major differential alterations in severe COVID-19. *iScience* 2023; **26**: 106260.

40 Ouk C, Roland L, Gachard N, Poulain S, Oblet C, Rizzo D *et al.* Continuous MYD88 Activation Is Associated With Expansion and Then Transformation of IgM Differentiating Plasma Cells. *Front Immunol* 2021; **12**: 641692.

41 Turchaninova MA, Davydov A, Britanova OV, Shugay M, Bikos V, Egorov ES *et al.* High-quality full-length immunoglobulin profiling with unique molecular barcoding. *Nat Protoc* 2016; **11**: 1599–1616.

42 Javaugue V, Pascal V, Bender S, Nasraddine S, Dargelos M, Alizadeh M *et al.* RNA-based immunoglobulin repertoire sequencing is a new tool for the management of monoclonal gammopathy of renal (kidney) significance. *Kidney Int* 2022; **101**: 331–337.

43 Boice M, Salloum D, Mourcin F, Sanghvi V, Amin R, Oricchio E *et al.* Loss of the HVEM Tumor Suppressor in Lymphoma and Restoration by Modified CAR-T Cells. *Cell* 2016; **167**: 405-418.e13.

44 Dobin A, Davis CA, Schlesinger F, Drenkow J, Zaleski C, Jha S *et al.* STAR: ultrafast universal RNA-seq aligner. *Bioinformatics* 2013; **29**: 15–21.

45 Liao Y, Smyth GK, Shi W. featureCounts: an efficient general purpose program for assigning sequence reads to genomic features. *Bioinformatics* 2014; **30**: 923–930.

46 Varet H, Brillet-Guéguen L, Coppée J-Y, Dillies M-A. SARTools: A DESeq2- and EdgeR-Based R Pipeline for Comprehensive Differential Analysis of RNA-Seq Data. *PLOS ONE* 2016; **11**: e0157022.

47 Wu T, Hu E, Xu S, Chen M, Guo P, Dai Z *et al.* clusterProfiler 4.0: A universal enrichment tool for interpreting omics data. *The Innovation* 2021; **2**: 100141.

48 Zhang X, Yoon HS, Chapdelaine-Williams AM, Kyritsis N, Alt FW. Physiological role of the 3'IgH CBEs super-anchor in antibody class switching. *Proc Natl Acad Sci U S A* 2021; **118**: e2024392118.

49 Hu J, Meyers RM, Dong J, Panchakshari RA, Alt FW, Frock RL. Detecting DNA double-stranded breaks in mammalian genomes by linear amplification-mediated high-throughput genome-wide translocation sequencing. *Nat Protoc* 2016; **11**: 853–871.

50 The Immunological Genome Project Consortium, Heng TSP, Painter MW, Elpek K, Lukacs-Kornek V, Mauermann N *et al.* The Immunological Genome Project: networks of gene expression in immune cells. *Nat Immunol* 2008; **9**: 1091–1094.

51 Yoshida H, Lareau CA, Ramirez RN, Rose SA, Maier B, Wroblewska A *et al.* The cis-Regulatory Atlas of the Mouse Immune System. *Cell* 2019; **176**: 897-912.e20.

52 Kohwi-Shigematsu T, Kohwi Y, Takahashi K, Richards HW, Ayers SD, Han H-J *et al.* SATB1-mediated functional packaging of chromatin into loops. *Methods San Diego Calif* 2012; **58**: 243–254.

53 Feng D, Chen Y, Dai R, Bian S, Xue W, Zhu Y *et al.* Chromatin organizer SATB1 controls the cell identity of CD4+ CD8+ double-positive thymocytes by regulating the activity of super-enhancers. *Nat Commun* 2022; **13**: 5554.

54 Zelenka T, Klonizakis A, Tsoukatou D, Papamatheakis D-A, Franzenburg S, Tzerpos P *et al.* The 3D enhancer network of the developing T cell genome is shaped by SATB1. *Nat Commun* 2022; **13**: 6954.

55 Dickinson LA, Dickinson CD, Kohwi-Shigematsu T. An Atypical Homeodomain in SATB1 Promotes Specific Recognition of the Key Structural Element in a Matrix Attachment Region. *J Biol Chem* 1997; **272**: 11463–11470.

56 Dickinson LA, Kohwi-Shigematsu T. Nucleolin is a matrix attachment region DNA-binding protein that specifically recognizes a region with high base-unpairing potential. *Mol Cell Biol* 1995; **15**: 456–465.

57 Marquet M, Garot A, Bender S, Carrion C, Rouaud P, Lecardeur S *et al.* The Eμ enhancer region influences H chain expression and B cell fate without impacting IgVH repertoire and immune response in vivo. *J Immunol Baltim Md 1950* 2014; **193**: 1171–1183.

58 Xu Y, Davidson L, Alt FW, Baltimore D. Deletion of the Ig kappa light chain intronic enhancer/matrix attachment region impairs but does not abolish V kappa J kappa rearrangement. *Immunity* 1996; **4**: 377–385.

59 Yi M, Wu P, Trevorrow KW, Claflin L, Garrard WT. Evidence that the Igkappa gene MAR regulates the probability of premature V-J joining and somatic hypermutation. *J Immunol Baltim Md 1950* 1999; **162**: 6029–6039.

60 Sakai E, Bottaro A, Davidson L, Sleckman BP, Alt FW. Recombination and transcription of the endogenous Ig heavy chain locus is effected by the Ig heavy chain intronic enhancer core region in the absence of the matrix attachment regions. *Proc Natl Acad Sci U S A* 1999; **96**: 1526–1531.

61 Garot A, Marquet M, Saintamand A, Bender S, Le Noir S, Rouaud P *et al.* Sequential activation and distinct functions for distal and proximal modules within the IgH 3' regulatory region. *Proc Natl Acad Sci U S A* 2016; **113**: 1618–1623.

62 Inlay M, Alt FW, Baltimore D, Xu Y. Essential roles of the kappa light chain intronic enhancer and 3' enhancer in kappa rearrangement and demethylation. *Nat Immunol* 2002; **3**: 463–468.

63 Bruzeau C, Moreau J, Le Noir S, Pinaud E. Panorama of stepwise involvement of the IgH 3' regulatory region in murine B cells. *Adv Immunol* 2021; **149**: 95–114.

64 Yokota T, Kanakura Y. Role of tissue-specific AT-rich DNA sequence-binding proteins in lymphocyte differentiation. *Int J Hematol* 2014; **100**: 238–245.

65 Satoh Y, Yokota T, Sudo T, Kondo M, Lai A, Kincade PW *et al.* The Satb1 protein directs hematopoietic stem cell differentiation toward lymphoid lineages. *Immunity* 2013; **38**: 1105–1115.

66 Martin OA, Thomas M, Marquet M, Bruzeau C, Garot A, Brousse M *et al.* The IgH Eμ-MAR regions promote UNG-dependent error-prone repair to optimize somatic hypermutation. *Front Immunol* 2023; **14**: 1030813.

67 Cumano A, Rajewsky K. Clonal recruitment and somatic mutation in the generation of immunological memory to the hapten NP. *EMBO J* 1986; **5**: 2459–2468.

68 Martin O, Thomas M, Marquet M, Garot A, Brousse M, Bender S *et al.* The IgH *Eμ* -MAR regions promote UNG-dependent error-prone repair to optimize somatic hypermutation. Immunology, 2022 doi:10.1101/2022.08.15.503996.

69 Reth M, Hämmerling GJ, Rajewsky K. Analysis of the repertoire of anti-NP antibodies in C57BL/6 mice by cell fusion. I. Characterization of antibody families in the primary and hyperimmune response. *Eur J Immunol* 1978; **8**: 393–400.

70 Fukita Y, Jacobs H, Rajewsky K. Somatic hypermutation in the heavy chain locus correlates with transcription. *Immunity* 1998; **9**: 105–114.

71 Zelenka T, Tzerpos P, Panagopoulos G, Tsolis KC, Papamatheakis D-A, Papadakis VM *et al.* SATB1 undergoes isoform-specific phase transitions in T cells. bioRxiv, 2022.

72 Kaur S, Coulombe Y, Ramdzan ZM, Leduy L, Masson J-Y, Nepveu A. Special AT-rich Sequence-binding Protein 1 (SATB1) Functions as an Accessory Factor in Base Excision Repair. *J Biol Chem* 2016; **291**: 22769–22780.

73 Winter DB, Phung QH, Zeng X, Seeberg E, Barnes DE, Lindahl T *et al.* Normal somatic hypermutation of Ig genes in the absence of 8-hydroxyguanine-DNA glycosylase. *J Immunol Baltim Md 1950* 2003; **170**: 5558–5562.

74 Kumar PP, Bischof O, Purbey PK, Notani D, Urlaub H, Dejean A *et al.* Functional interaction between PML and SATB1 regulates chromatin-loop architecture and transcription of the MHC class I locus. *Nat Cell Biol* 2007; **9**: 45–56.

75 Tan J-AT, Sun Y, Song J, Chen Y, Krontiris TG, Durrin LK. SUMO conjugation to the matrix attachment region-binding protein, special AT-rich sequence-binding protein-1 (SATB1), targets SATB1 to promyelocytic nuclear bodies where it undergoes caspase cleavage. *J Biol Chem* 2008; **283**: 18124–18134.

76 Zhang Y, Zhang X, Dai H-Q, Hu H, Alt FW. The role of chromatin loop extrusion in antibody diversification. *Nat Rev Immunol* 2022; **22**: 550–566.

Legend to Figures

Figure 1.

A) Conditional deletion of *Satb1*-exon 4 by *Cd79a*$^{cre/+}$ recombinase in B cells. Exon 4, cre site, frt site, conditional allele (*Satb1*^{flx}) and Wild type allele (*Satb1*$^{+}$) are indicated. **B)** SATB1 protein quantification by Western Blot in splenic B cells from WT (*Satb1*$^{flx/+}$), conditional heterozygous (*Satb1*$^{flx/+}$ *Cd79a*$^{cre/+}$) and conditional homozygous (*Satb1*$^{flx/flx}$ *Cd79a*$^{cre/+}$) mice. **C)** *Satb1* transcript quantification by RT-qPCR (normalized to *Hprt*) in Peyer's patch naive and GC B cells sorted from WT mice (n=8) from 3 independent experiments. **D)** Bar graphs displaying absolute numbers of B cell subsets determined by flow cytometry from bone marrow (per femur, n=7-10) and spleen (n=11-15) from 4-5 independent experiments. **E)** Pie chart representation of *IgHV* family gene usage, quantified by RACE-RepSeq, expressed by pre-B cell-enriched bone marrow populations in WT (n=5) and cKO mice (n=6) from 2 independent experiments. **F)** Immunoglobulin serum isotype levels quantified by ELISA in 8 to 10 week-old WT and cKO mice (n=8-15) from 4 independent experiments. Error bars represent SEM; p-value was determined with two tailed Mann Whitney test; non-significant (ns) and significant differences are indicated (*** p<0.001).

Figure 2.

A) Comparison of surface IgM fluorescence intensity, evaluated by flow cytometry, on immature and recirculating bone marrow B cell subsets from two-month-old WT and homozygous cKO animals. One representative histogram is shown (left), bar graph (right) displays normalized surface IgM MFI in WT and cKO animals (n=7-10 from 4 independent experiments). **B**) Comparison of surface IgM fluorescence intensity, evaluated by flow cytometry, on Follicular (FO), Marginal zone (MZ), Transitional (Tr.1, Tr.2, Tr.3) splenic B cell subsets from two-month-old WT and homozygous cKO animals. One representative histogram is shown (left), bar graph (right) displays normalized surface IgM MFI in WT and cKO animals (n=13-14 from 5 independent experiments). **C**) Comparison of surface IgM fluorescence intensity, evaluated by flow cytometry, on naive B cells sorted from Peyer's Patches from two-month-old WT and homozygous cKO animals. One representative histogram is shown (left), bar graph (right) display normalized surface IgM MFI in WT and cKO animals (n=10-11 from 3 independent experiments). **D**) *IgH* and *Igκ* primary transcripts quantified by RT-qPCR (normalized to *Hprt*) in splenic resting B cells sorted from WT and cKO mice (n= 6-10 from 5 independent experiments). **E**) Volcano plot from RNA-seq indicating differentially expressed transcripts when comparing WT and cKO mice (n=2) resting B cells. Transcripts located within Ig gene loci are indicated. Error bars represent SEM; p-value was determined by two tailed Mann Whitney test; non-significant (ns) and significant differences are indicated (* p<0.05; ** p<0.01; *** p<0.001; **** p<0.0001).

Figure 3.

A) Visual representation of Gene Ontology enrichment analysis of genes significantly associated with biological pathways upon B cell transition from resting (day 0) to *in vitro*-activated (day 2) subsets in WT and cKO mice. Datasets from RNA-seq experiments were used for the analysis. **B**) Same representation as above for B cell transition from *in vitro*-activated (day 2) to plasmablast (day 4) subsets. **C**) Germinal center (GC) B cell subsets evaluated by flow cytometry in Peyer's patches of WT and cKO animals (n=12-18 from 4 independent experiments). **D**) Comparison of surface IgM fluorescence intensity evaluated by flow cytometr, on Peyer's patch GC B cells from two-month-old WT and homozygous cKO animals. One representative histogram is shown (left), bar graph (right) displays normalized surface IgM MFI in WT and cKO animals (n=10-11 from 3 independent experiments) **E**) Proportion of plasmablasts evaluated by flow cytometry, obtained following *in vitro* LPS activation (day 4) of splenic B cells from WT and cKO animals (n=13-18 from 6 independent experiments) (left). **F**) Proportion of plasma cells in the spleen evaluated by flow cytometry following NP-CGG immunization of WT and cKO animals (n=6-7 from 1 experiment). **G**) Comparison of intracellular IgM fluorescence intensity evaluated by flow cytometry, in *in vitro*-differentiated plasmablasts (day4) from WT and homozygous cKO animals. One representative histogram is shown (left), bar graph (right) displays normalized intracellular IgM MFI in WT and cKO animals (n=9-10 from 4 independent experiments). **H**) *IgH* and *Igκ* primary transcripts quantified by RT-qPCR (normalized to *Hprt*) in *in vitro* LPS-activated B-lineage cells (day 4) of WT and cKO animals (n=9-13 from 5 independent experiments). **J**) Volcano plots from RNA-seq indicating differentially expressed transcripts when comparing WT and cKO mice (n=2) in *in vitro* LPS-activated B cells (day 2). Transcripts located within Ig gene V regions are indicated. **K**) Same analysis as above in *in vitro* LPS-differentiated plasmablasts (day 4). Error bars represent SEM; p-value was determined by two tailed Mann Whitney test; non-significant (ns) and significant differences were indicated (* $p<0.05$; ** $p<0.01$).

Figure 4.

Comparison of primary transcription and somatic hypermutation in WT and cKO animals, taking place in various regions of Ig genes targeted by AID (left schemas), in spontaneous GC B cells sorted from Peyer's patches (n=7-10 from 4 independent experiments, left and middle bar graphs). Somatic hypermutation in splenic GC B cells sorted after NP-CGG immunization (n=7-8 from 4 independent experiments, right bar graphs). Data were obtained by NGS (Ion proton) combined with DeMinEr filtering, an accurate dedicated method to quantify AID-induced substitutions in B-lineage cells (50). **A**) Transcription and SHM upstream from *IgH Sμ* region. **B**) Transcription and SHM within the *IgH* intron downstream from *VJ558* (consensus) to J_H4-rearranged exons (in spontaneous GC B cells) or in the same region downstream from *V186.2* to J_H4-rearranged exons (in NP-CGG-induced GC B cells). **C**) Transcription and SHM within the *Igk* intron downstream from

all-rearranged *Jκ5* segments. Error bars represent SEM; p-value was determined by two tailed Mann Whitney test; non-significant (ns) and significant differences were indicated (* $p<0.05$).

Fig. 1

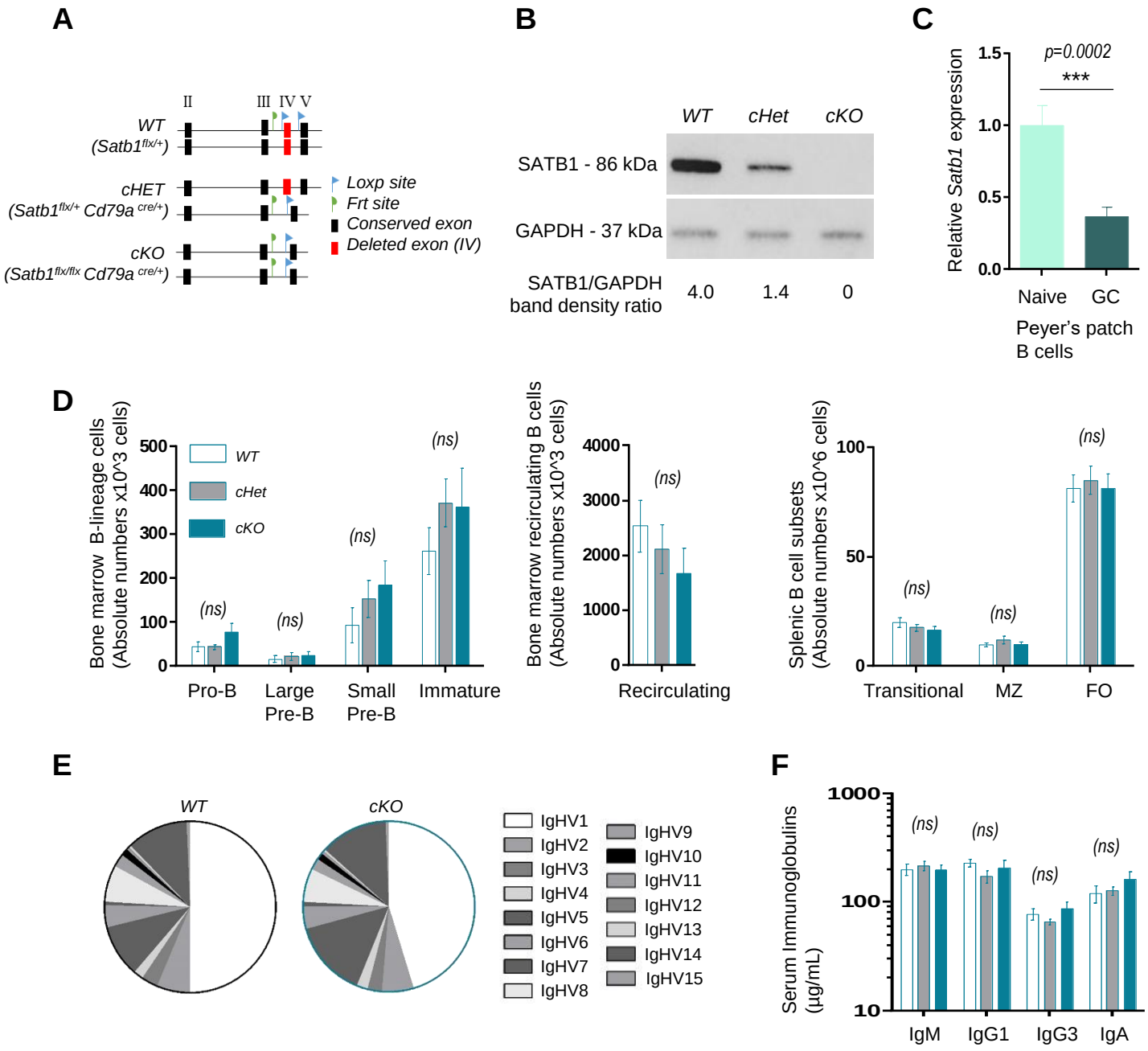
A
II
III IV V
WT
(Satb1flx/+)
cHET
(Satb1flx/+ Cd79a cre/+)
cKO
(Satb1flx/flx Cd79a cre/+)
Loxp site
Frt site
Conserved exon
Deleted exon (IV)
B
WT
cHet
cKO
SATB1 - 86 kDa
GAPDH - 37 kDa
SATB1/GAPDH band density ratio
4.0
1.4
0
C
p=0.0002
***
Relative Satb1 expression
1.5
1.0
0.5
0.0
Naive
GC
Peyer's patch B cells
D
Bone marrow B-lineage cells (Absolute numbers x10^3 cells)
500
400
300
200
100
0
WT
cHet
cKO
(ns)
Pro-B
Large Pre-B
Small Pre-B
Immature
Bone marrow recirculating B cells (Absolute numbers x10^3 cells)
4000
3000
2000
1000
0
Recirculating
Splenic B cell subsets (Absolute numbers x10^6 cells)
100
50
0
Transitional
MZ
FO
E
WT
cKO
IgHV1
IgHV2
IgHV3
IgHV4
IgHV5
IgHV6
IgHV7
IgHV8
IgHV9
IgHV10
IgHV11
IgHV12
IgHV13
IgHV14
IgHV15
F
Serum Immunoglobulins (µg/mL)
1000
100
10
IgM
IgG1
IgG3
IgA

Fig. 2

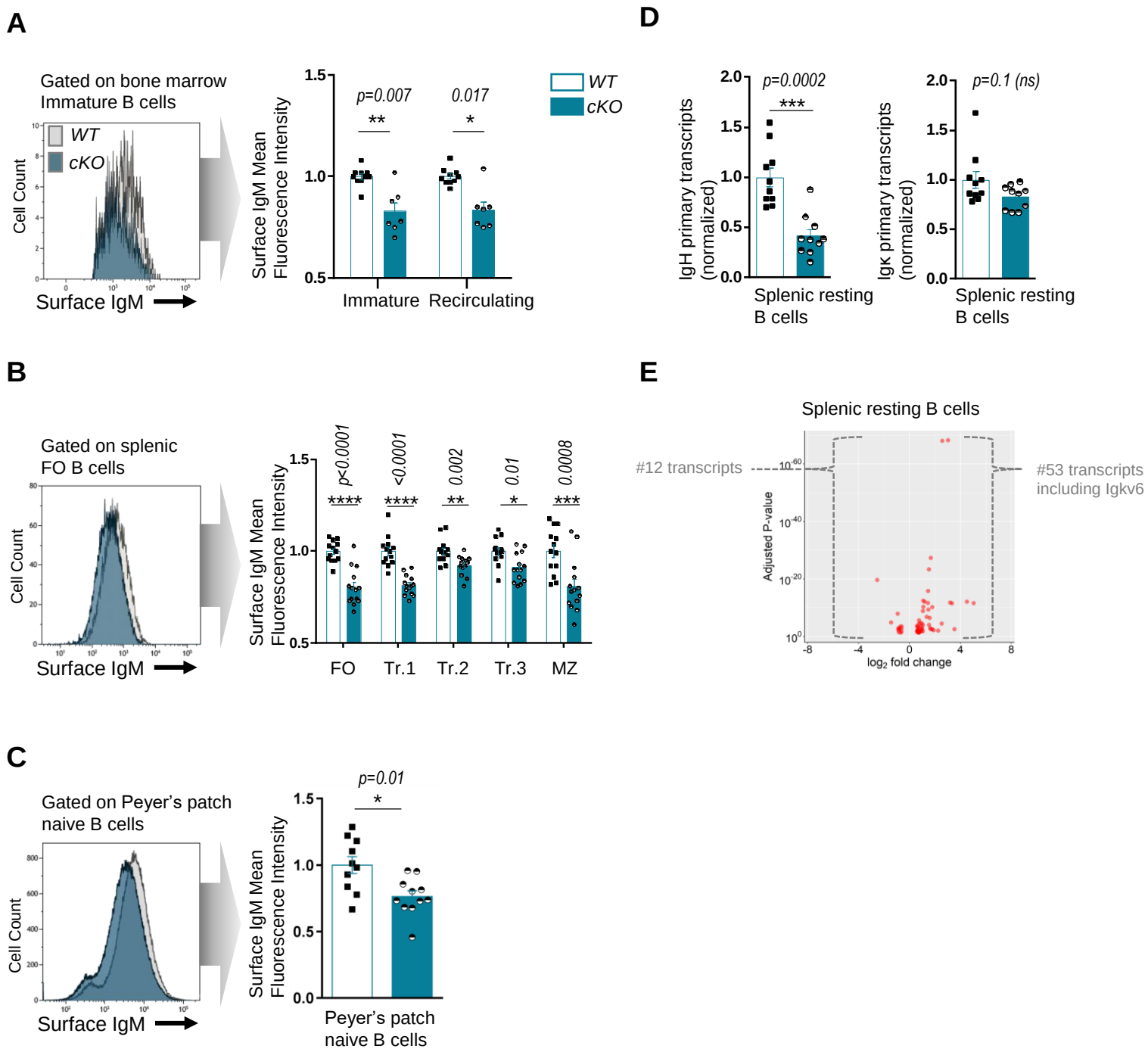
A
Gated on bone marrow
Immature B cells
WT
cKO
Cell Count
Surface IgM
Surface IgM Mean
Fluorescence Intensity
p=0.007
0.017
**
*
Immature
Recirculating
D
IgH primary transcripts
(normalized)
p=0.0002
***
Splenic resting
B cells
Igκ primary transcripts
(normalized)
p=0.1 (ns)
B
Gated on splenic
FO B cells
p<0.0001
<0.0001
0.002
0.01
0.0008
****
****
**
*
***
FO
Tr.1
Tr.2
Tr.3
MZ
E
Splenic resting B cells
#12 transcripts
#53 transcripts
including Igkv6
Adjusted P-value
log2 fold change
C
Gated on Peyer's patch
naive B cells
p=0.01
*
Peyer's patch
naive B cells

Fig. 3

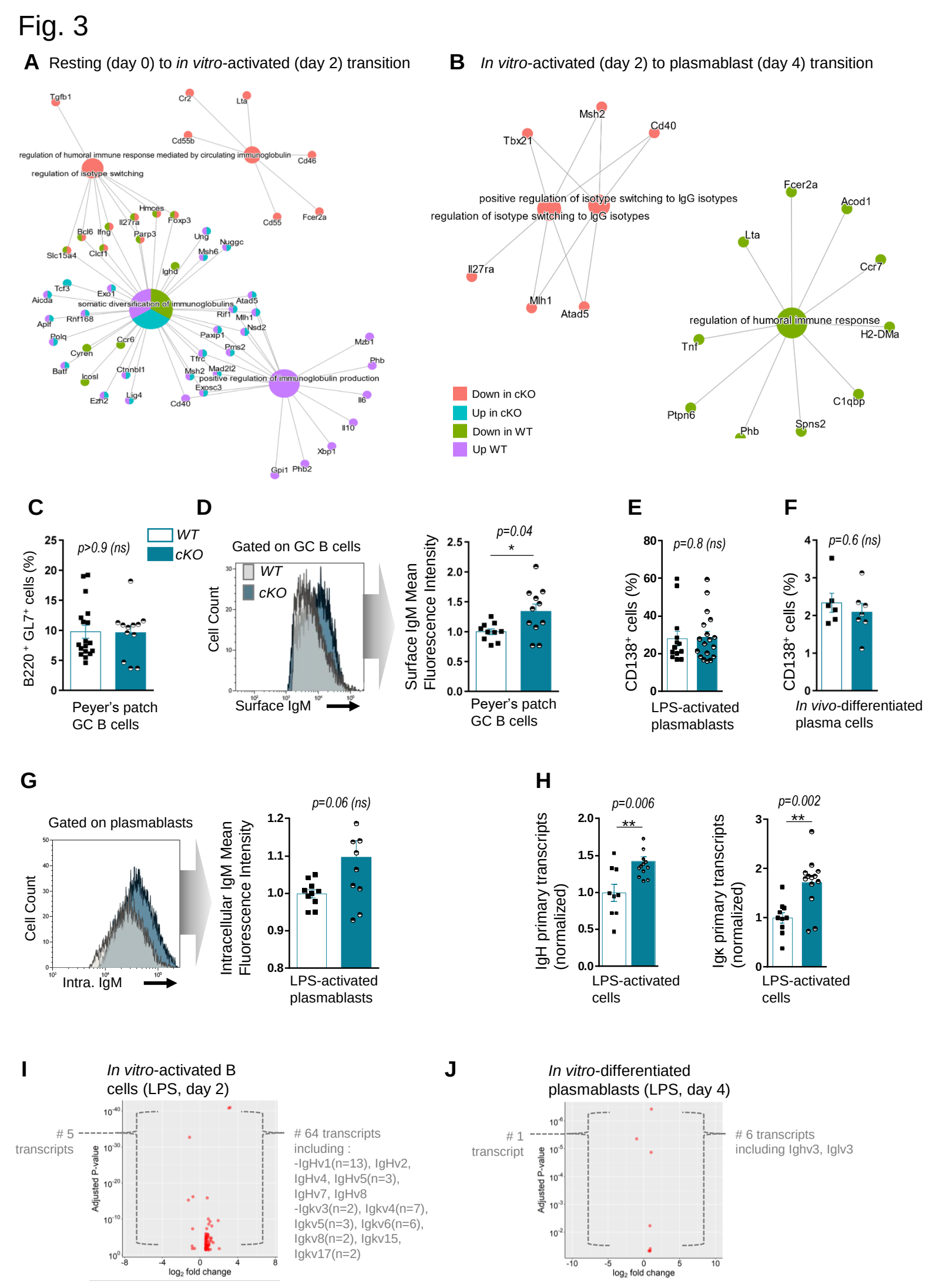
A Resting (day 0) to in vitro-activated (day 2) transition
B In vitro-activated (day 2) to plasmablast (day 4) transition
Tgfb1
Cr2
Lta
Cd55b
regulation of humoral immune response mediated by circulating immunoglobulin
Cd46
regulation of isotype switching
Hmces
Il27ra
Foxp3
Cd55
Fcer2a
Bcl6
Ifng
Parp3
Ung
Nuggc
Slc15a4
Clcf1
Msh6
Ighd
Tcf3
Exo1
Aicda
somatic diversification of immunoglobulins
Atad5
Rif1
Mlh1
Rnf168
Apif
Nsd2
Polq
Paxip1
Ccr6
Pms2
Mzb1
Cyren
Tfrc
Phb
Batf
Msh2
Mad2l2
Ctnnbl1
positive regulation of immunoglobulin production
Icosl
Exosc3
Lig4
Ezh2
Cd40
Il6
Il10
Xbp1
Gpi1
Phb2
Msh2
Cd40
Tbx21
positive regulation of isotype switching to IgG isotypes
regulation of isotype switching to IgG isotypes
Il27ra
Mlh1
Atad5
Fcer2a
Acod1
Lta
Ccr7
regulation of humoral immune response
H2-DMa
Tnf
C1qbp
Ptpn6
Phb
Spns2
Down in cKO
Up in cKO
Down in WT
Up WT
C
D
E
F
WT
cKO
p>0.9 (ns)
B220+ GL7+ cells (%)
Peyer's patch GC B cells
Gated on GC B cells
Cell Count
Surface IgM
p=0.04
*
Surface IgM Mean Fluorescence Intensity
Peyer's patch GC B cells
p=0.8 (ns)
CD138+ cells (%)
LPS-activated plasmablasts
p=0.6 (ns)
CD138+ cells (%)
In vivo-differentiated plasma cells
G
H
Gated on plasmablasts
Cell Count
Intra. IgM
p=0.06 (ns)
Intracellular IgM Mean Fluorescence Intensity
LPS-activated plasmablasts
p=0.006
**
IgH primary transcripts (normalized)
LPS-activated cells
p=0.002
**
Igκ primary transcripts (normalized)
LPS-activated cells
I
In vitro-activated B cells (LPS, day 2)
5 transcripts
Adjusted P-value
log2 fold change
64 transcripts including :
-IgHv1(n=13), IgHv2, IgHv4, IgHv5(n=3), IgHv7, IgHv8
-Igkv3(n=2), Igkv4(n=7), Igkv5(n=3), Igkv6(n=6), Igkv8(n=2), Igkv15, Igkv17(n=2)
J
In vitro-differentiated plasmablasts (LPS, day 4)
1 transcript
Adjusted P-value
log2 fold change
6 transcripts including Ighv3, Iglv3

Fig. 4

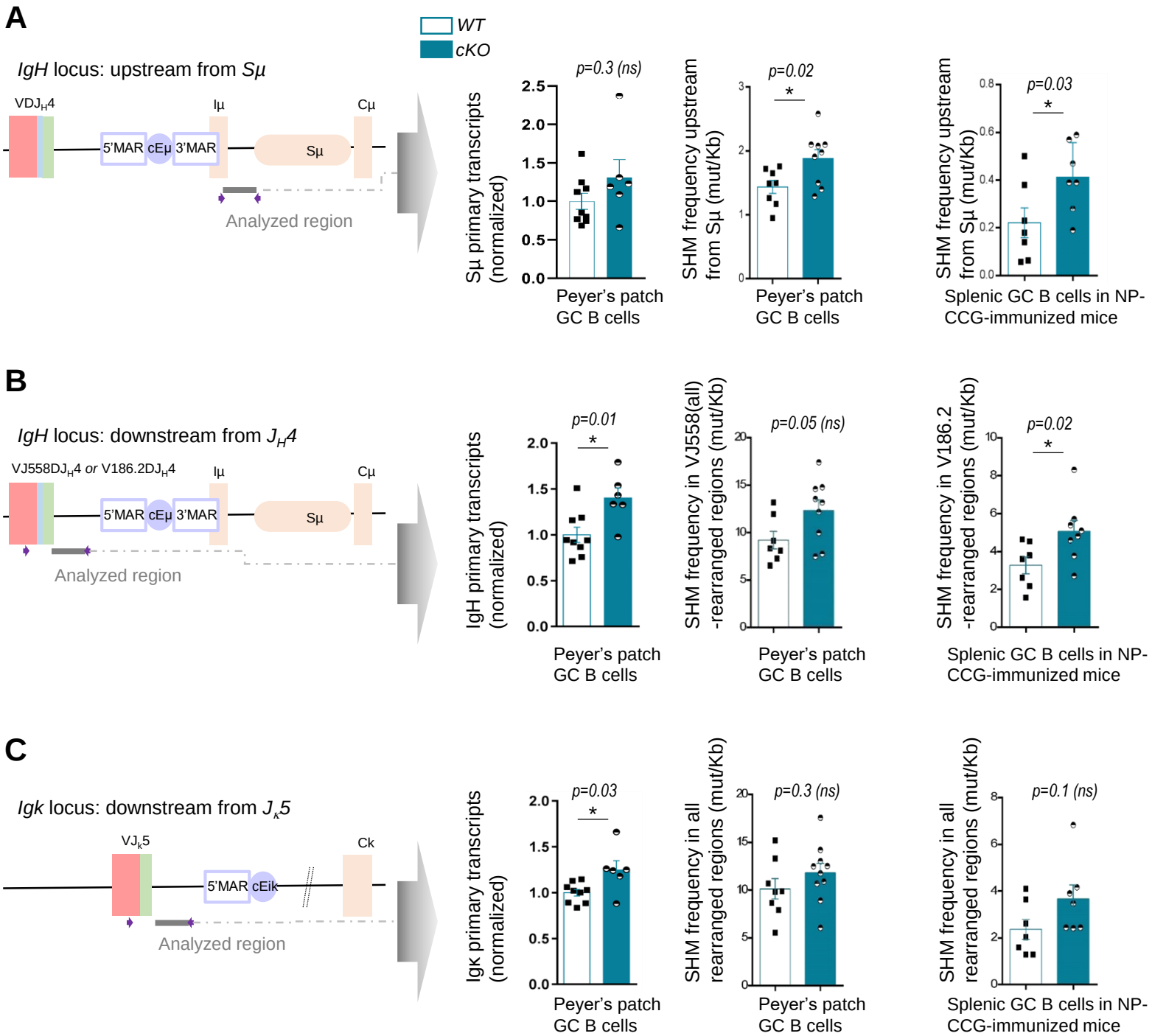
A
WT
cKO
IgH locus: upstream from Sμ
VDJH4
Iμ
Cμ
5'MAR cEμ 3'MAR
Sμ
Analyzed region
Sμ primary transcripts (normalized)
p=0.3 (ns)
Peyer's patch GC B cells
SHM frequency upstream from Sμ (mut/Kb)
p=0.02
*
Peyer's patch GC B cells
SHM frequency upstream from Sμ (mut/Kb)
p=0.03
*
Splenic GC B cells in NP-CCG-immunized mice
B
IgH locus: downstream from JH4
VJ558DJH4 or V186.2DJH4
Iμ
Cμ
5'MAR cEμ 3'MAR
Sμ
Analyzed region
IgH primary transcripts (normalized)
p=0.01
*
Peyer's patch GC B cells
SHM frequency in VJ558(all) -rearranged regions (mut/Kb)
p=0.05 (ns)
Peyer's patch GC B cells
SHM frequency in V186.2 -rearranged regions (mut/Kb)
p=0.02
*
Splenic GC B cells in NP-CCG-immunized mice
C
Igk locus: downstream from Jκ5
VJk5
Ck
5'MAR cEik
Analyzed region
Igk primary transcripts (normalized)
p=0.03
*
Peyer's patch GC B cells
SHM frequency in all rearranged regions (mut/Kb)
p=0.3 (ns)
Peyer's patch GC B cells
SHM frequency in all rearranged regions (mut/Kb)
p=0.1 (ns)
Splenic GC B cells in NP-CCG-immunized mice

Fig. S1

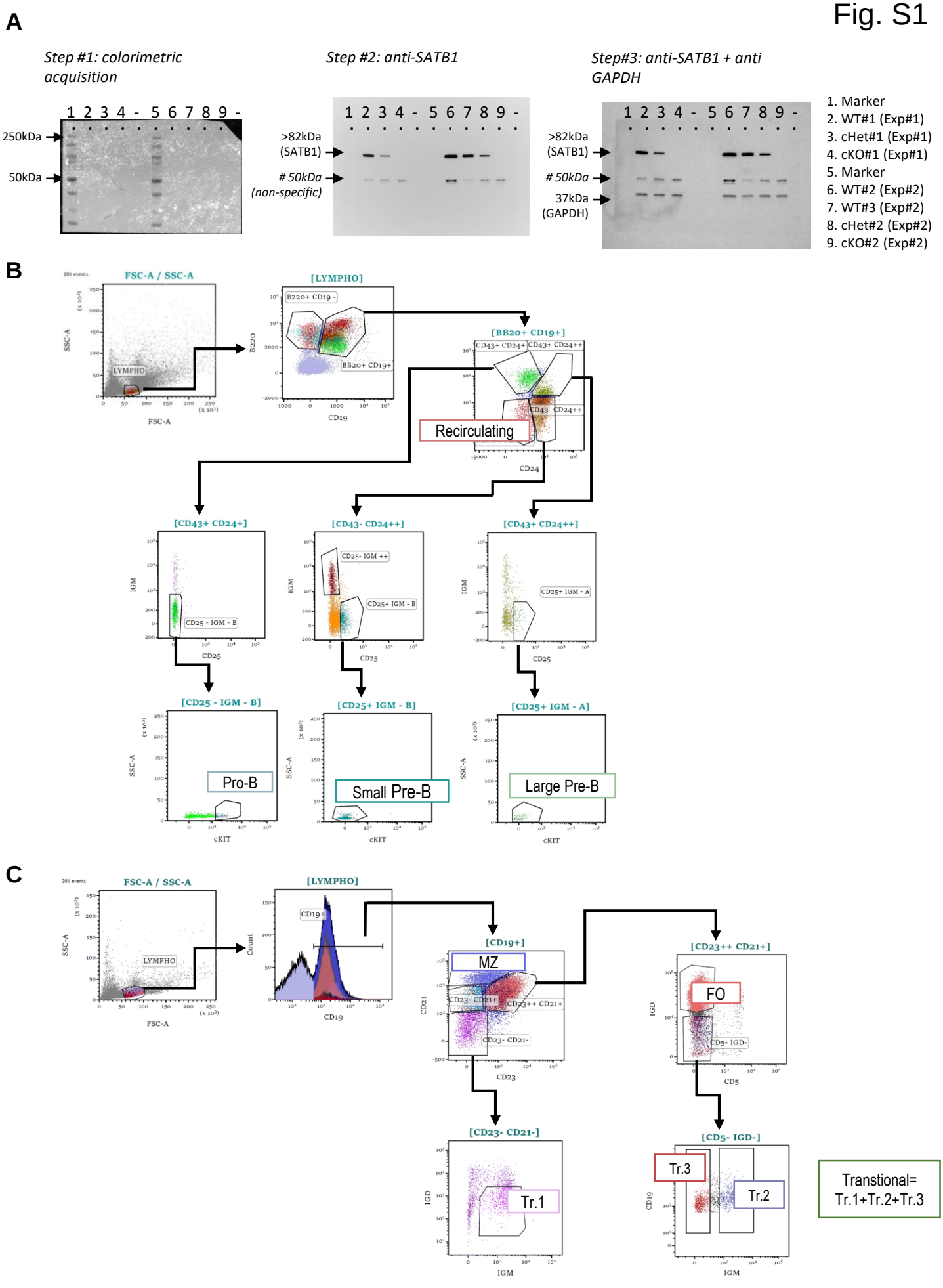

Fig. S1. ***(A)*** Unprocessed original images of Western blots quantifying SATB1 protein expression in sorted splenic B cells from WT, cKO heterozygous and cKO homozygous mice. ***(B)*** Gating Strategy used to analyse bone marrow mouse B cell subsets in Fig.1D. ***(C)*** Same as *(B)* for B cell subsets from the spleen.

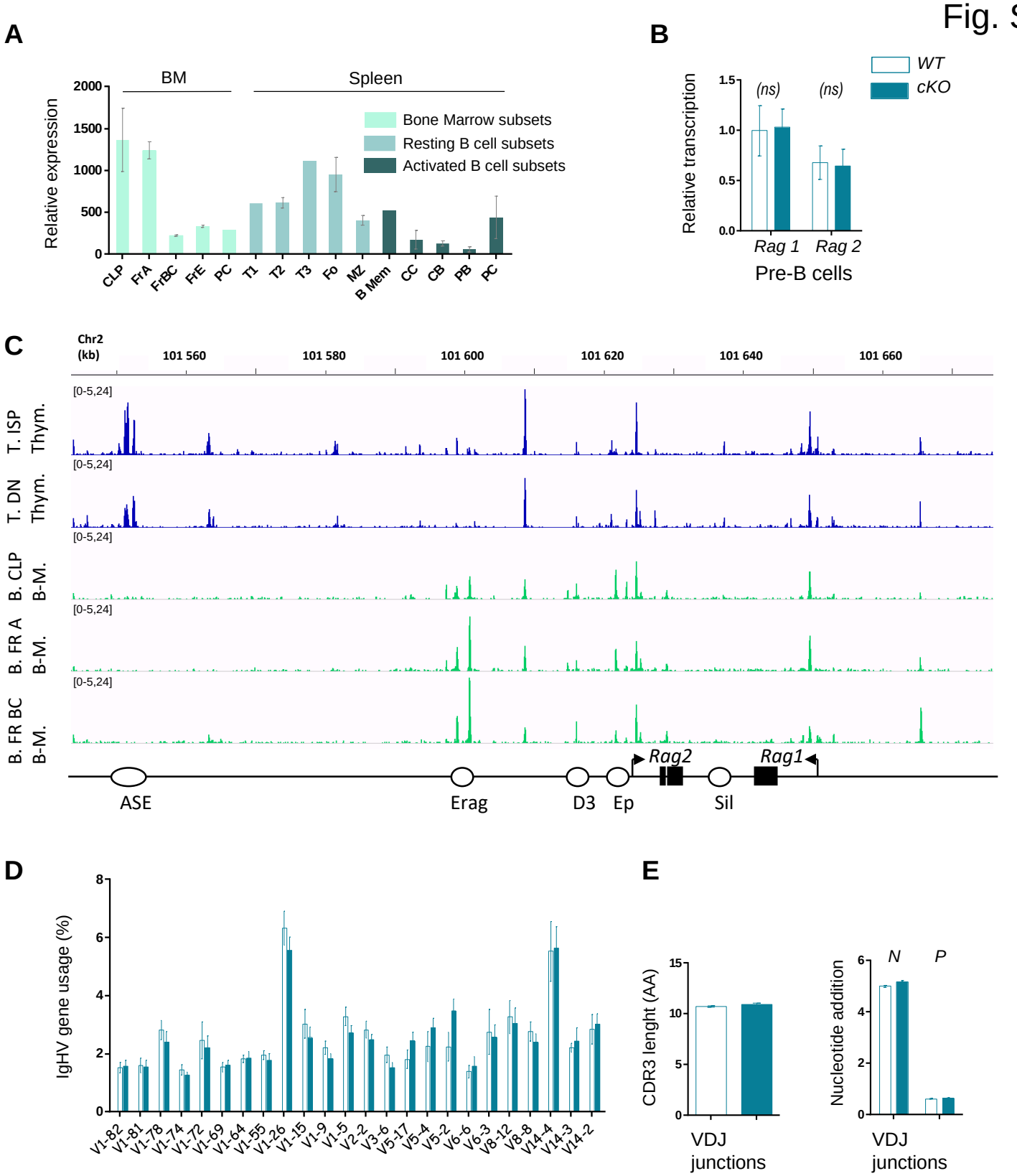

Figure S2. ***(A)*** Representation of SATB1 relative expression in murine *wt* B cell populations with Gene Skyline data browser (ImmGen ULI RNASeq data group[46]). Populations include Common Lymphoid progenitor, Hardy fractions A, B, C, E and mature peripheral B cell subsets. ***(B)*** Transcription of *Rag1* and *Rag2* genes quantified in bone marrow sorted pre-B cells from wt (n=6) and *Satb1* cKO (n=5) mice. Error bars represent SEM; p-value was determined with two tailed Mann Whitney test. ***(C)*** Comparison of *Rag* gene loci accessibility by ATAC-seq in thymocytes (intermediate single-positive and double positive populations, upper lanes in blue) and bone-marrow developing B cells (common lymphoid progenitor, fractions A and BC, lower lanes in green) performed in wt mice, published data assembled by the ImmGen consortium[46, 47] , relevant regulatory elements are indicated. ***(D)*** Comparison of *IgHV* gene relative proportion, quantified by RACE-RepSeq, expressed by pre-B cell-enriched bone marrow populations in wt (n=5) and cKO mice (n=6). ***(E)*** Comparison of CDR3 length (left panel), N and P-nucleotide addition (right panel) during VDJ recombination for wt (n=5) and cKO mice (n=6). Statistical analysis was not performed given the minor differences observed.

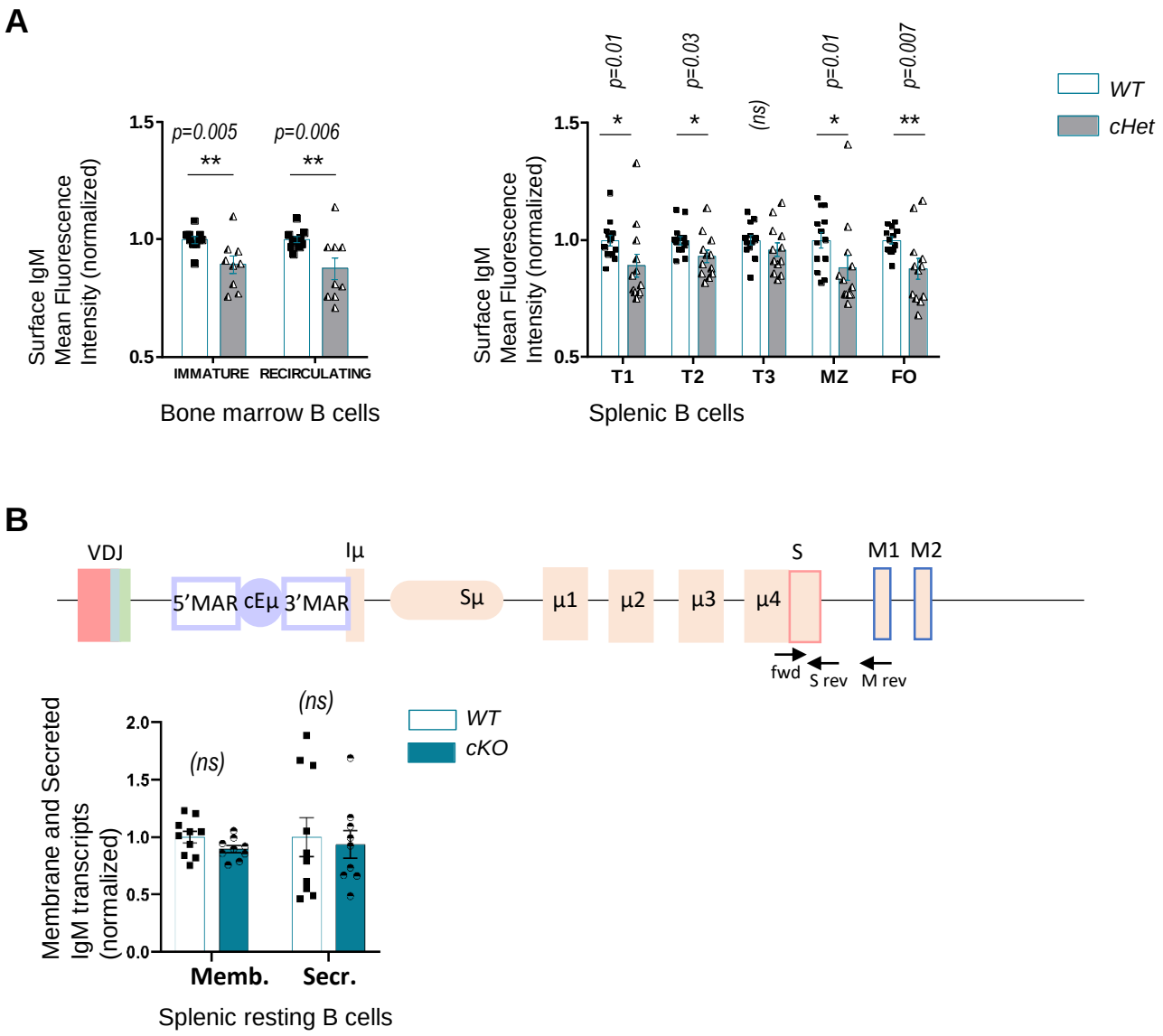

Fig. S3. ***(A)*** Mean Fluorescence Intensity measured by FACS analysis (normalized on WT samples) of IgM expressed at the surface of B cell subsets of 2-month-old WT and cKO heterozygous mice. Left panel includes data from bone marrow IgM expressing B cell subsets (n=7-9). Right panel includes data from B cell subset from the spleen (n=12-13). ***(B)*** Primer location to quantify Membrane and Secreted IgM transcripts on the mouse IgH locus (top, not to scale), RT-qPCR quantification (Normalized to *Hprt*) in splenic resting B cells of WT (n=10) and cKO (n=9) animals. Error bars represent SEM; p-value was determined by two tailed Mann Whitney test; non-significant (ns) and significant differences are indicated (* $p<0.05$; ** $p<0.01$).

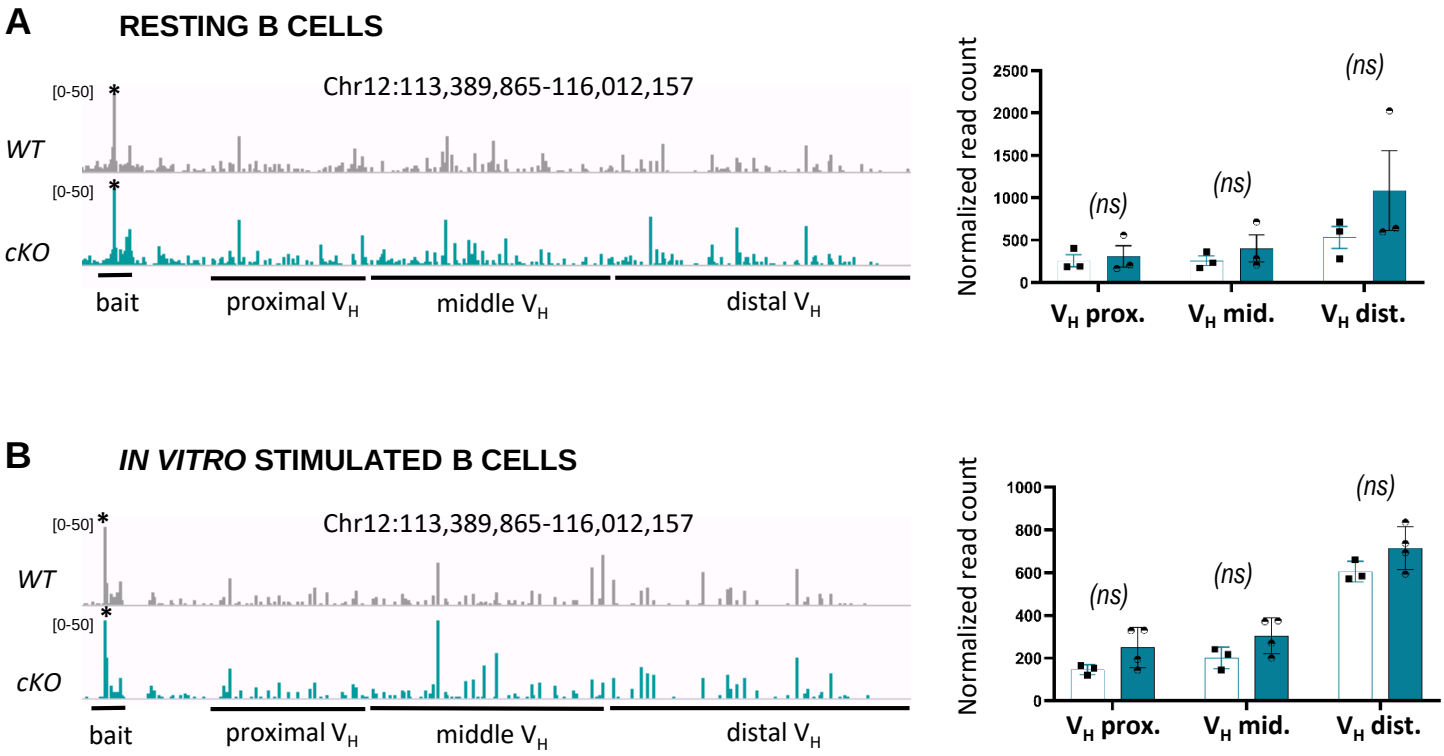

Fig. S4. ***(A)*** Chromatin loops in resting B cells from spleen (n=3 of each genotype). Intrachromosomal interactions at IgH locus measured by 3C HTGTS between the bait located close to *Eμ* enhancer (*IμSμ* region) and the V_H family regions in B cells from WT and cKO mice (> 2-month-old). Left diagram: representative bedgraph of each genotype (IGV browser), showing physical interaction between bait (identified by an asterisk) and the various V_H segments (proximal, middle and distal) positioned on the germline locus. Right diagram display normalized coverage reads mapping with respective V_H family regions from 3 to 4 sample of each genotype.. ***(B)*** Same as *(A)* in LPS-activated B cells for 3 days (n=3-4 of each genotype). Error bars represent SEM; p-value was determined by two tailed Mann Whitney test; non-significant (ns) differences are indicated.

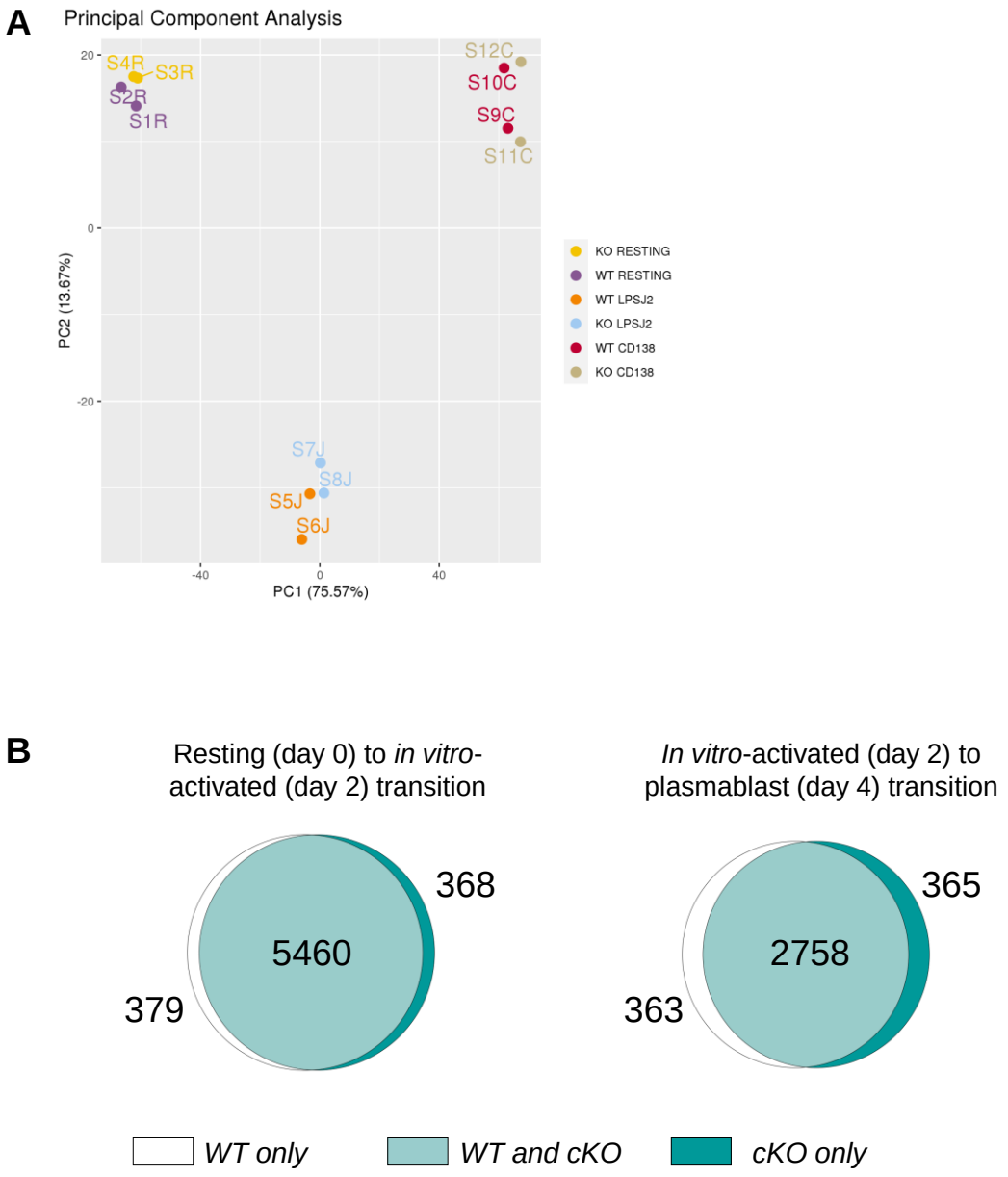

Fig. S5. ***(A)*** Principal Component Analysis of RNA sequencing of resting (R), LPS stimulated (J) or plasmablast (C) cells from WT and cKO mice (n=2). ***(B)*** Venn diagrams from RNA-seq displaying numbers and proportions of differentially expressed transcripts of B-lineage cells from WT and cKO mice (n=2) during resting to *in vitro*-activated (day 2) transition (left) and during *in vitro*-activated to plasmablast (day 4) transition (right)

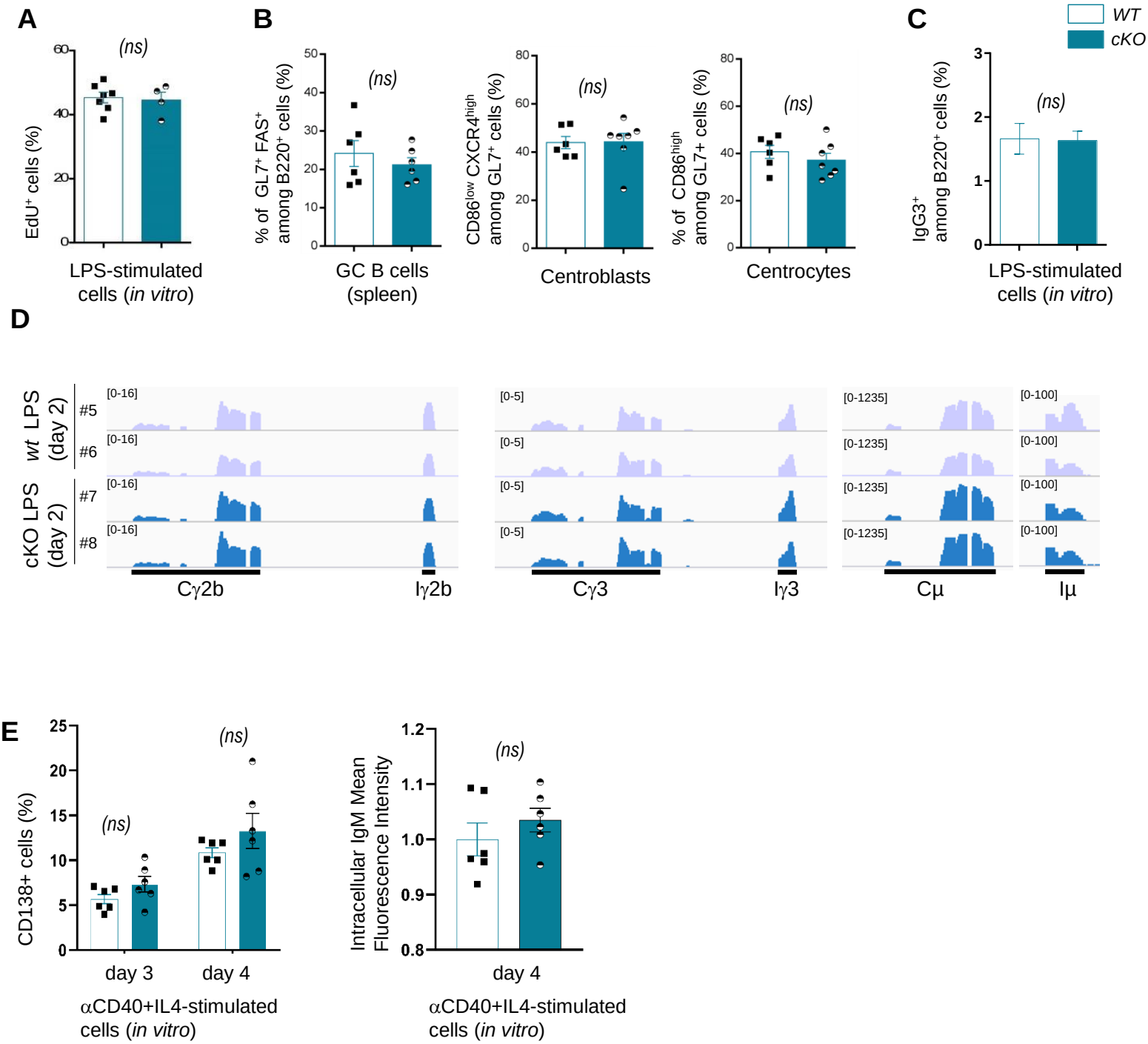

Fig. S6. ***(A)*** Percentage of EdU-incorporating splenic B cells from WT and cKO mice during *in vitro* LPS activation (n=4-7). ***(B)*** Detailed analysis of germinal center (GC) populations obtained following NP-CGG immunization of WT (n=6) and cKO (n=7) animals: percentage of GC B cells ($B220^{+}GL7^{+}$, left) among splenic B cells, percentage of centroblasts ($CD86^{Low}CXCR4^{High}$, upper right) & centrocytes ($CD86^{High}$, lower right) within the initial GC B cell subset. ***(C)*** IgG3 switched cells obtained after *in vitro* activation of splenic B cells with LPS at day 4. ***(D)*** Visual representation of relevant *IgH* constant gene transcripts induced in *in vitro* LPS-activated B cells (day 2) from WT and cKO mice (n=2). Bedgraph files from RNAseq analysis were aligned on mouse GRCm38/mm10 assembly using IGV browser. ***(E)*** Proportion of plasmablasts evaluated by flow cytometry, obtained following *in vitro* αCD40+IL4 activation (day 3 and day 4) of splenic B cells from WT and cKO animals (left); Comparison of intracellular IgM fluorescence intensity evaluated by flow cytometry, in *in vitro*-differentiated plasmablasts (αCD40+IL4, day4) from WT and homozygous cKO animals (n=6). Error bars represent SEM; p-value was determined by two tailed Mann Whitney test; non-significant (ns) differences are indicated.

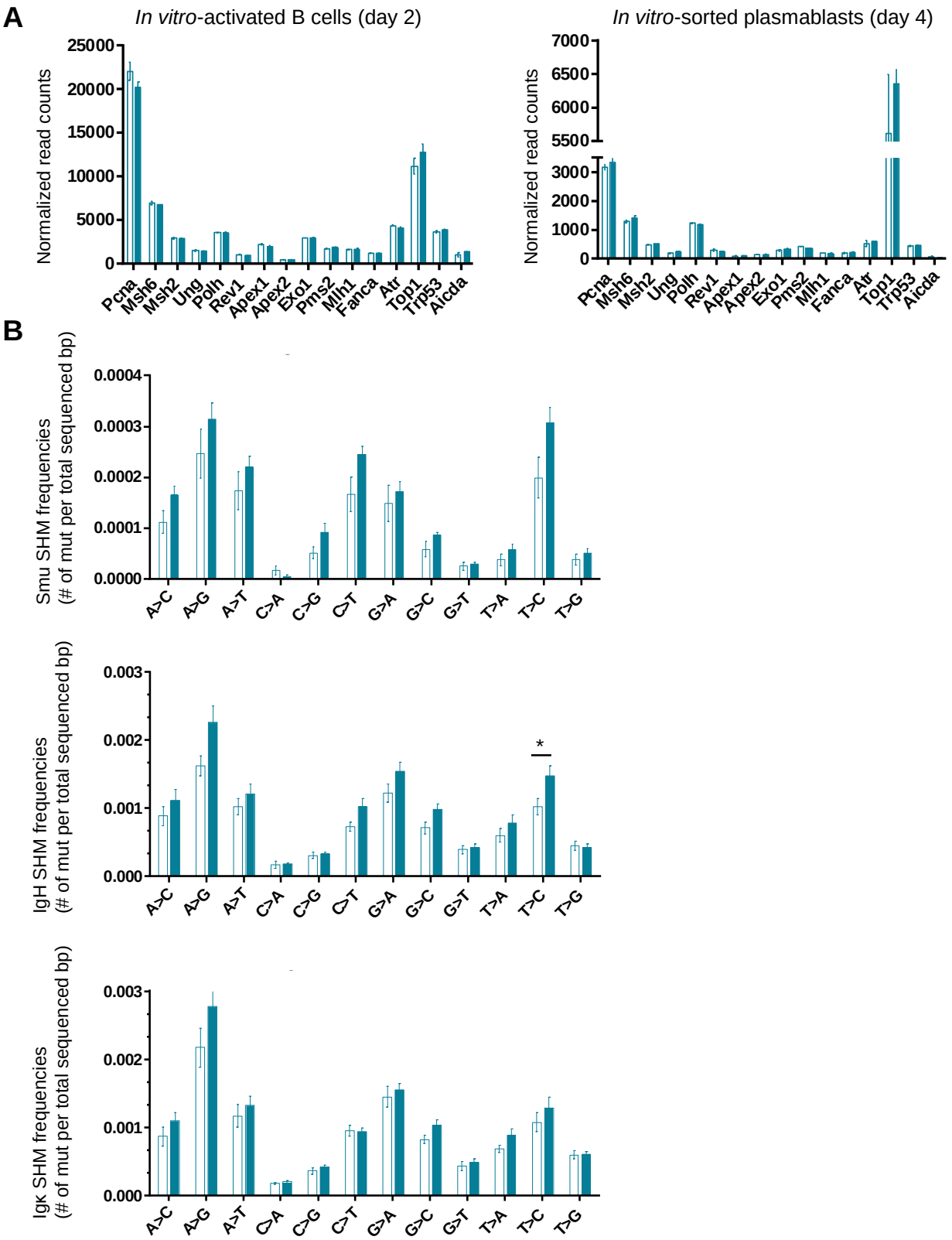

Fig. S7. ***(A)*** Relative expression of genes involved in SHM and SHM-associated DNA repair pathways in *in vitro* activated B cell- (day 2) or enriched-plasma cell- (day 4) subsets of WT and cKO mice evaluated by RNA-seq (n=2). ***(B)*** Base substitution patterns, reported in frequencies for each base, in GC B cells sorted from Peyer's patches of WT and cKO mice. SHM taking place within the region upstream from *IgH Sμ* (top), downstream from rearranged-J_H4 exons (middle) and downstream from rearranged-*Jk5* exons (bottom) (n=7-10). Data were obtained by NGS (Ion proton) combined to DeMinEr filtering. Error bars represent SEM; p-value was determined with two tailed Mann Whitney test, only significant differences were indicated (* $p<0.05$).

Supplementary Table S1: summary table of genotyping primers

Primer name	Sequence	Gene
EF	5'-TTTGCTCATGTGGAATGTCGAGGTA-3'	Satb1
KR	5'-GGGCAAGAACATAAAGTGACCCTC-3'C	Satb1
EF2	5'-AATAATCTGCTCCACTGCTCCACTGAGGACCCAC-3'	Satb1
ER3	5'-CCCTATTGCAGTGGGAATCAGCAT-3'	Satb1
MB1 CRE Wild Type Forward	5'-CTCTTTACCTTCCAAGCACTGA-3'	Mb1
MB1 CRE COMMON	5'-ACTGAGGCAGGAGGATTGG-3'	Mb1
MB1 CRE MUTANT Forward	5-'CATTTTCGAGGGAGCTTCA-3'	Mb1

Supplementary Table S2: antibodies used for Western blot, ELISA and flow cytometry

	Antibody	Clone	Dilution	Sources
WESTERN BLOT	SATB1	EPR3951	1/1000	ABCAM AB109122
	GAPDH	AF5718	1/5000	RD SYSTEMS
	Goat anti-rabbit	AB_2632593	1/5000	SOUTHERNBIOTECH
ELISA	Unlabeled Goat Anti Mouse IgM	1020-01	1/500	SOUTHERNBIOTECH
	Unlabeled Goat Anti Mouse IgG1	1070-01	1/500	SOUTHERNBIOTECH
	Unlabeled Goat Anti Mouse IgG3	1100-01	3/1000	SOUTHERNBIOTECH
	Unlabeled Goat Anti Mouse IgA	1040-01	1/250	SOUTHERNBIOTECH
	Goat Anti Mouse IgM-AP	1021-04	1/1000	SOUTHERNBIOTECH
	Goat Anti Mouse IgG1-AP	1070-04	1/1000	SOUTHERNBIOTECH
	Goat Anti Mouse IgG3-AP	1100-04	1/1000	SOUTHERNBIOTECH
	Goat Anti Mouse IgA-AP	1040-04	1/1000	SOUTHERNBIOTECH
Flow cytometry BONE MARROW B CELLS	cKIT BV421	2B8	1/100	BECTON DICKINSON 562609
	B220 BV510	RA3-6B2	1/100	BIOLEGEND 103248
	CD25 APC	PC61	1/100	BECTON DICKINSON 561048
	CD24 FITC	M2/169	1/100	BECTON DICKINSON 553261
	CD43 PE	S7	1/100	BECTON DICKINSON PHARM 553271
	IGM PC7	II /41	1/100	EBIOSCIENCE 25-5790-82
	CD19 APCH7	1D3	1/100	BECTON DICKINSON PHARM 560143
Flow cytometry SPLENIC B CELLS	CD5 FITC	53-7.3	1/100	BECTON DICKINSON 5530211
	CD19 APCH7	1D3	1/100	BECTON DICKINSON PHARM 560143
	CD23 PC7	B3B4	1/100	BIOLEGEND 101614
	CD21 PE	7G6	1/100	BECTON DICKINSON PHARM 552957
	IGM APC	II /41	1/100	EBIOSCIENCE 17-2590-82
	IGD BV421	11-26C-2A	1/100	BIOLEGEND 405725
Flow cytometry PEYER ‘S PATCHES CELLS	B220 APC	RA3-6B2	1/100	BIOLEGEND 103212
	GL7 FITC	GL7	1/100	BECTON DICKINSON 553666
Flow cytometry CENTROCYTE / CENTROBLAST	B220 BV510	RA3-6B2	1/100	BIOLEGEND 103248
	CD38 FITC	90	1/100	BECTON DICKINSON 558813
	FAS BV421	Jo2	1/100	BECTON DICKINSON 562633
	CXCR4 PE	2B11/CXCR4	1/50	BECTON DICKINSON PHARM 551966
	CD86 APC	GL1	1/50	BIOLEGEND 105011
Flow Cytometry *IN VITRO* STIMULATED CELLS	B220 BV421	RA3-6B2	1/100	BECTON DICKINSON 562922
	IGM PC7	II/41	1/100	EBIOSCIENCE 25-5790-82
	IgG3 FITC	R40-82	1/100	BECTON DICKINSON 553403
	CD138 APC	281-2	1/100	BECTON DICKINSON 558626

Supplementary Table S3: List of Gene Ontology pathway used

GO:0031296	GO:0019731	GO:0002759	GO:0006958	GO:0019731	GO:0061844	GO:0019731	GO:0006956	GO:0001869	GO:0002803
GO:0002344	GO:0019732	GO:0061844	GO:0002455	GO:0001867	GO:0006958	GO:0061844	GO:0006958	GO:0001971	GO:0006958
GO:0002352	GO:0061844	GO:0006958	GO:0006958	GO:0061844	GO:0061844	GO:0019731	GO:0006956	GO:0045916	GO:0002455
GO:0002344	GO:0019731	GO:0061844	GO:0002455	GO:0006958	GO:0006958	GO:0006958	GO:0006958	GO:0061844	GO:0019731
GO:0002352	GO:0006959	GO:0019731	GO:0019731	GO:0019731	GO:0061844	GO:0031296	GO:0019731	GO:0002759	GO:0006958
GO:0002344	GO:0006958	GO:0061844	GO:0002455	GO:0061844	GO:0019731	GO:0002344	GO:0019732	GO:0061844	GO:0002455
GO:0016446	GO:0019730	GO:0019731	GO:0019731	GO:0019731	GO:0002780	GO:0002352	GO:0061844	GO:0006958	GO:0006958
GO:0006959	GO:0002455	GO:0061844	GO:0002455	GO:0061844	GO:0002759	GO:0002344	GO:0019731	GO:0061844	GO:0002455
GO:0006956	GO:0019731	GO:0019731	GO:0006958	GO:0019731	GO:0002786	GO:0002352	GO:0006959	GO:0019731	GO:0019731
GO:0002922	GO:0061844	GO:0061844	GO:0002455	GO:0061844	GO:0019731	GO:0002344	GO:0006958	GO:0061844	GO:0002455
GO:0019731	GO:0019731	GO:0006959	GO:0006958	GO:0019731	GO:0006958	GO:0016446	GO:0019730	GO:0019731	GO:0019731
GO:0019732	GO:0006958	GO:0002925	GO:0002455	GO:0006959	GO:0001869	GO:0006959	GO:0002455	GO:0061844	GO:0002455
GO:0061844	GO:0045916	GO:0006959	GO:0006958	GO:0019731	GO:0006958	GO:0006956	GO:0019731	GO:0019731	GO:0006958
GO:0019731	GO:0045959	GO:0061844	GO:0002455	GO:0061844	GO:0045916	GO:0002922	GO:0061844	GO:0061844	GO:0002455
GO:0019732	GO:0006956	GO:0019732	GO:0006958	GO:0019731	GO:0006958	GO:0019731	GO:0019731	GO:0006959	GO:0006958
GO:0061844	GO:0045916	GO:0019731	GO:0002455	GO:0002760	GO:0019731	GO:0019732	GO:0006958	GO:0002925	GO:0002455
GO:0019731	GO:0030449	GO:0006956	GO:0006958	GO:0002779	GO:0019732	GO:0061844	GO:0045916	GO:0006959	GO:0006958
GO:0061844	GO:0006958	GO:0002925	GO:0002455	GO:0002780	GO:0061844	GO:0019731	GO:0045959	GO:0061844	GO:0002455
GO:0019731	GO:0043152	GO:0002815	GO:0019731	GO:0006958	GO:0019731	GO:0019732	GO:0006956	GO:0019732	GO:0006958
GO:0019732	GO:0061844	GO:0006963	GO:0061844	GO:0061844	GO:0002455	GO:0061844	GO:0045916	GO:0019731	GO:0002455
GO:0061844	GO:0001867	GO:0006965	GO:0019731	GO:0006959	GO:0006958	GO:0019731	GO:0030449	GO:0006956	GO:0006958
GO:0002803	GO:0045916	GO:0006958	GO:0061844	GO:0061844	GO:0019731	GO:0061844	GO:0006958	GO:0002925	GO:0002455
GO:0019731	GO:0001867	GO:0002925	GO:0002925	GO:0006957	GO:0002455	GO:0019731	GO:0043152	GO:0002815	GO:0019731
GO:0061844	GO:0006957	GO:0006958	GO:0006958	GO:0019731	GO:0019731	GO:0019732	GO:0061844	GO:0006963	GO:0061844
GO:0019731	GO:0006958	GO:0019731	GO:0061844	GO:0061844	GO:0002455	GO:0061844	GO:0001867	GO:0006965	GO:0019731
GO:0061844	GO:0045959	GO:0061844	GO:0006957	GO:0019731	GO:0006958	GO:0002803	GO:0045916	GO:0006958	GO:0061844
GO:0006958	GO:0006957	GO:0006959	GO:0006958	GO:0006956	GO:0019731	GO:0019731	GO:0001867	GO:0002925	GO:0002925
GO:0061844	GO:0006959	GO:0006958	GO:0006956	GO:0030449	GO:0006956	GO:0061844	GO:0006957	GO:0006959	GO:0006958
GO:0006958	GO:0043152	GO:0019731	GO:0019731	GO:0030451	GO:0006957	GO:0019731	GO:0006958	GO:0019731	GO:0061844
GO:0006956	GO:0061844	GO:0061844	GO:0019732	GO:0006956	GO:0006958	GO:0061844	GO:0045959	GO:0061844	GO:0006957
GO:0030449	GO:0002924	GO:0019731	GO:0061844	GO:0030449	GO:0019731	GO:0006958	GO:0006957	GO:0006959	GO:0006958
GO:0030451	GO:0006959	GO:0061844	GO:0019731	GO:0006956	GO:0061844	GO:0061844	GO:0006959	GO:0006958	GO:0006956
GO:0006956	GO:0061844	GO:0006959	GO:0006958	GO:0006957	GO:0019731	GO:0006958	GO:0043152	GO:0019731	GO:0019731
GO:0006957	GO:0001971	GO:0061844	GO:0061844	GO:0061844	GO:0002812	GO:0006956	GO:0061844	GO:0061844	GO:0019732
GO:0006956	GO:0045916	GO:0019731	GO:0019731	GO:0001867	GO:0001867	GO:0030449	GO:0002924	GO:0019731	GO:0061844
GO:0001905	GO:0001971	GO:0061844	GO:0061844	GO:0061844	GO:0061844	GO:0030451	GO:0006959	GO:0061844	GO:0019731
GO:0006956	GO:0030449	GO:0002925	GO:0019731	GO:0002923	GO:0006958	GO:0006956	GO:0061844	GO:0006959	GO:0006958
GO:0006957	GO:0001971	GO:0006959	GO:0006958	GO:0002925	GO:0006959	GO:0006957	GO:0001971	GO:0061844	GO:0061844
GO:0006956	GO:0061844	GO:0002925	GO:0045916	GO:0030449	GO:0061844	GO:0006956	GO:0045916	GO:0019731	GO:0019731
GO:0030449	GO:0006958	GO:0006959	GO:0045959	GO:0045957	GO:0019731	GO:0001905	GO:0001971	GO:0061844	GO:0061844
GO:0061844	GO:0019731	GO:0019731	GO:0030449	GO:0045959	GO:0061844	GO:0006956	GO:0030449	GO:0002925	GO:0019731
GO:0002920	GO:0061844	GO:0019732	GO:0030450	GO:0045957	GO:0019731	GO:0006957	GO:0001971	GO:0006959	GO:0006958
GO:0006958	GO:0006958	GO:0061844	GO:0006958	GO:0061844	GO:0061844	GO:0006956	GO:0061844	GO:0002925	GO:0045916
GO:0006959	GO:0061844	GO:0019731	GO:0045916	GO:0002786	GO:0019731	GO:0030449	GO:0006958	GO:0006959	GO:0045959
GO:0061844	GO:0019731	GO:0061844	GO:0045959	GO:0006959	GO:0061844	GO:0061844	GO:0019731	GO:0019731	GO:0030449
GO:0006958	GO:0061844	GO:0019731	GO:0061844	GO:0061844	GO:0019731	GO:0002920	GO:0061844	GO:0019732	GO:0030450
GO:0006957	GO:0019731	GO:0006958	GO:0019731	GO:0019731	GO:0061844	GO:0006958	GO:0006958	GO:0061844	GO:0006958
GO:0006958	GO:0061844	GO:0061844	GO:0045959	GO:0061844	GO:0019731	GO:0006959	GO:0061844	GO:0019731	GO:0045916
GO:0006956	GO:0006958	GO:0019731	GO:0061844	GO:0006959	GO:0061844	GO:0061844	GO:0019731	GO:0061844	GO:0045959
GO:0006958	GO:0002803	GO:0006958	GO:0019731	GO:0019731	GO:0019731	GO:0006958	GO:0061844	GO:0019731	GO:0061844
GO:0002920	GO:0061844	GO:0002787	GO:0019732	GO:0006958	GO:0061844	GO:0006957	GO:0019731	GO:0006958	GO:0019731
GO:0019731	GO:0006958	GO:0061844	GO:0061844	GO:0019731	GO:0019731	GO:0006958	GO:0061844	GO:0061844	GO:0045959
GO:0061844	GO:0061844	GO:0002225	GO:0019731	GO:0019732	GO:0061844	GO:0006956	GO:0006958	GO:0019731	GO:0061844
GO:0019731	GO:0006958	GO:0006959	GO:0061844	GO:0061844	GO:0019731	GO:0006958	GO:0002803	GO:0006958	GO:0019731
GO:0061844	GO:0002455	GO:0019731	GO:0019731	GO:0006958	GO:0061844	GO:0002920	GO:0061844	GO:0002787	GO:0019732
GO:0006956	GO:0006959	GO:0019732	GO:0006959	GO:0030449	GO:0019731	GO:0019731	GO:0006958	GO:0061844	GO:0061844
GO:0006957	GO:0006958	GO:0061844	GO:0006958	GO:0006958	GO:0061844	GO:0061844	GO:0061844	GO:0002225	GO:0019731
GO:0006958	GO:0006959	GO:0019731	GO:0061844	GO:0061844	GO:0019731	GO:0019731	GO:0006958	GO:0006959	GO:0061844
GO:0006956	GO:0019731	GO:0045959	GO:0006958	GO:0006958	GO:0061844	GO:0061844	GO:0002455	GO:0019731	GO:0019731
GO:0006957	GO:0061844	GO:0006958	GO:0006956	GO:0006959	GO:0019731	GO:0006956	GO:0006959	GO:0019732	GO:0006959
GO:0006958	GO:0019731	GO:0001867	GO:0061844	GO:0061844	GO:0006959	GO:0006957	GO:0006958	GO:0061844	GO:0006958
GO:0006956	GO:0006956	GO:0006958	GO:0006958	GO:0006959	GO:0006958	GO:0006958	GO:0006959	GO:0019731	GO:0061844
GO:0001970	GO:0006957	GO:0001867	GO:0061844	GO:0019730	GO:0043152	GO:0006956	GO:0019731	GO:0045959	GO:0006958
GO:0006956	GO:0006958	GO:0006958	GO:0019730	GO:0045960	GO:0001867	GO:0006957	GO:0061844	GO:0006958	GO:0006956
GO:0045917	GO:0030451	GO:0001867	GO:0061844	GO:0061844	GO:0006956	GO:0006958	GO:0019731	GO:0001867	GO:0061844
GO:0006956	GO:0006956	GO:0002786	GO:0019731	GO:0006958	GO:0019730	GO:0006956	GO:0006956	GO:0006958	GO:0006958
GO:0006958	GO:0019732	GO:0045917	GO:0061844	GO:0002455	GO:0019732	GO:0001970	GO:0006957	GO:0001867	GO:0061844
GO:0045959	GO:0061844	GO:0006958	GO:0019731	GO:0006956	GO:0006958	GO:0006956	GO:0006958	GO:0006958	GO:0019730
GO:0006956	GO:0045959	GO:0006959	GO:0006958	GO:0002925	GO:0006959	GO:0045917	GO:0030451	GO:0001867	GO:0061844
GO:0001970	GO:0061844	GO:0019731	GO:0002922	GO:0061844	GO:0061844	GO:0006956	GO:0006956	GO:0002786	GO:0019731
GO:0006956	GO:0043152	GO:0061844	GO:0002924	GO:0019731	GO:0006958	GO:0006958	GO:0019732	GO:0045917	GO:0061844
GO:0006957	GO:0019731	GO:0006958	GO:0006959	GO:0061844	GO:0045917	GO:0045959	GO:0061844	GO:0006958	GO:0019731
GO:0006958	GO:0061844	GO:0019731	GO:0006958	GO:0006958	GO:0061844	GO:0006956	GO:0045959	GO:0006959	GO:0006958
GO:0030449	GO:0043152	GO:0006959	GO:0006959	GO:0045957	GO:0002924	GO:0001970	GO:0061844	GO:0019731	GO:0002922
GO:0030451	GO:0006958	GO:0006958	GO:0061844	GO:0001867	GO:0006958	GO:0006956	GO:0043152	GO:0061844	GO:0002924
GO:0006956	GO:0001869	GO:0002803	GO:0019732	GO:0019731	GO:0002225	GO:0006957	GO:0019731	GO:0006958	GO:0006959
GO:0006958	GO:0001971	GO:0006958	GO:0001867	GO:0019732	GO:0030449	GO:0006958	GO:0061844	GO:0019731	GO:0006958
GO:0006956	GO:0045916	GO:0002455	GO:0006958	GO:0061844	GO:0006958	GO:0030449	GO:0043152	GO:0006959	GO:0006959
GO:0006958	GO:0061844	GO:0019731	GO:0001867	GO:0006958	GO:0006959	GO:0030451	GO:0006958	GO:0006958	GO:0061844

GO:0019732	GO:0030451	GO:0002639	GO:0002377	GO:0002639	GO:0048294	GO:0002377	GO:0002377	GO:0016446	GO:0002377
GO:0001867	GO:0006956	GO:0045830	GO:0002381	GO:0048295	GO:0048302	GO:0002639	GO:0002381	GO:0002204	GO:0048289
GO:0006958	GO:0030449	GO:0002638	GO:0002377	GO:0045830	GO:0045191	GO:2000572	GO:0002344	GO:0045190	GO:0048294
GO:0001867	GO:0006956	GO:0045190	GO:0048298	GO:0045190	GO:0002426	GO:0045830	GO:0002381	GO:0016447	GO:0002377
GO:0019731	GO:0006957	GO:0002377	GO:0002639	GO:0048304	GO:0002377	GO:0048304	GO:0002377	GO:0016446	GO:0045190
GO:0001867	GO:0061844	GO:0002637	GO:0002377	GO:0002377	GO:0033152	GO:0002377	GO:0016446	GO:0002381	GO:0002638
GO:0061844	GO:0001867	GO:0048304	GO:0002638	GO:0002381	GO:0002381	GO:0002639	GO:0002377	GO:0002377	GO:0002639
GO:0006958	GO:0061844	GO:0002377	GO:0002377	GO:0002639	GO:0002377	GO:0002377	GO:0002637	GO:0002637	GO:0002377
GO:0019731	GO:0002923	GO:0002637	GO:0002208	GO:0002638	GO:0002639	GO:0048302	GO:0002377	GO:0002381	GO:0045190
GO:0061844	GO:0002925	GO:0048304	GO:0045830	GO:0016446	GO:0045830	GO:0045830	GO:0045190	GO:0002377	GO:0002377
GO:0019731	GO:0030449	GO:0002377	GO:0002377	GO:0002637	GO:0045190	GO:0002208	GO:0002377	GO:0002638	GO:0016446
GO:0061844	GO:0045957	GO:0002639	GO:0045190	GO:0016445	GO:0002639	GO:0045830	GO:0002381	GO:0002639	GO:0033152
GO:0019731	GO:0045959	GO:0048304	GO:0002208	GO:0002377	GO:0002377	GO:0048298	GO:0002638	GO:0002638	GO:0045191
GO:0061844	GO:0045957	GO:0002639	GO:0045830	GO:0045190	GO:0002639	GO:0048304	GO:0002639	GO:0002377	GO:0002377
GO:0019731	GO:0061844	GO:0002638	GO:0002377	GO:0045830	GO:0048304	GO:0002204	GO:0002377	GO:0016446	GO:0002639
GO:0006959	GO:0002786	GO:0033152	GO:0016446	GO:0002381	GO:0048295	GO:0016447	GO:0016445	GO:0048298	GO:0002377
GO:0019731	GO:0006959	GO:0002377	GO:0016447	GO:0016446	GO:0048304	GO:0045190	GO:0016446	GO:0048304	GO:0002344
GO:0061844	GO:0061844	GO:0033152	GO:0045190	GO:0002637	GO:0048295	GO:0016447	GO:0045190	GO:0016446	GO:0002377
GO:0019731	GO:0019731	GO:0045190	GO:0016447	GO:0002381	GO:0002639	GO:0016446	GO:0002639	GO:0016447	GO:0002639
GO:0002760	GO:0061844	GO:0033152	GO:0002377	GO:0002638	GO:0048304	GO:0016447	GO:0048302	GO:0016446	GO:0048298
GO:0002779	GO:0006959	GO:0048290	GO:0045191	GO:0033152	GO:0002639	GO:0002204	GO:0048294	GO:0002377	GO:0071707
GO:0002780	GO:0019731	GO:0016446	GO:0045190	GO:0045190	GO:0048289	GO:0016446	GO:0048289	GO:0048298	GO:0002377
GO:0006958	GO:0006958	GO:0045190	GO:0045830	GO:0033152	GO:0048291	GO:0045190	GO:0002637	GO:0002426	GO:0045830
GO:0061844	GO:0019731	GO:0016447	GO:0016446	GO:0002377	GO:0002639	GO:0016446	GO:0002639	GO:0002381	GO:0002377
GO:0006959	GO:0019732	GO:0016446	GO:0002381	GO:0045190	GO:0048304	GO:0002639	GO:0048304	GO:0002377	GO:0048304
GO:0061844	GO:0061844	GO:0045190	GO:0002377	GO:0045830	GO:0002639	GO:0002377	GO:0002377	GO:0045190	GO:0002377
GO:0006957	GO:0006958	GO:0002377	GO:0016447	GO:0048302	GO:0002377	GO:0048298	GO:0016445	GO:0016446	GO:0002381
GO:0019731	GO:0030449	GO:0002638	GO:0016446	GO:0002377	GO:0002637	GO:0002639	GO:0071707	GO:0002377	GO:0002377
GO:0061844	GO:0048289	GO:0002377	GO:0002377	GO:0048297	GO:0002344	GO:0002377	GO:0016446	GO:0002639	GO:0002639
GO:0019731	GO:0048295	GO:0002381	GO:0071707	GO:0002377	GO:0016446	GO:2000558	GO:0002377	GO:0045829	GO:0002377
GO:0006956	GO:0002377	GO:0048304	GO:0048304	GO:0002208	GO:0002377	GO:0002377	GO:0048298	GO:0002637	GO:0002319
GO:0030449	GO:0033152	GO:0002344	GO:0016446	GO:0045830	GO:2000558	GO:0002381	GO:0048304	GO:0048291	GO:0002906

Supplementary Table S4: List of differentially expressed genes in resting B cells

Genes downregulated in resting B cells						
MGI SYMBOL	**WT**	**cKO**	**FoldChange**	**log2FoldChange**	**pvalue**	**padj**
Hspa1a	188896	122130	0.647	-0.629	4.58040337476548e-6	0.00191077385433822
Hspd1	49936	32268	0.646	-0.63	5.29346297269999e-7	2.9673168376341e-4
Tnf	1570	1008	0.642	-0.64	9.48629703355245e-5	0.0215398982516283
Snord118	627	392	0.625	-0.679	2.595515118942e-4	0.0484982814620647
Hspe1	33980	20312	0.598	-0.742	8.0046597154752e-7	4.1025024564626e-4
Ccrl2	1730	998	0.576	-0.796	5.81615734952946e-6	0.00231844956746354
Oasl1	2640	1502	0.569	-0.814	4.34376907467054e-6	0.00185520308717715
Rnu5g	502	282	0.558	-0.842	1.734644340325e-4	0.0366071178550015
Map3k19	765	416	0.546	-0.873	2.03195896221967e-5	0.00662714179350843
Bag3	1758	955	0.543	-0.881	3.20931750492121e-6	0.00143921843508192
Xlr3b	754	276	0.367	-1.447	1.74137977854962e-8	1.35812480294013e-5
Ifi208	826	141	0.172	-2.542	6.32098751900608e-24	2.2677174823186198e-20

Genes upregulated in resting B cells						
MGI SYMBOL	**WT**	**cKO**	**FoldChange**	**log2FoldChange**	**pvalue**	**padj**
Abca6	34	119	3.443	1.784	8.34323187989419e-6	0.00305430394819474
Abca8b	52	158	3.075	1.621	2.99174456038325e-6	0.00137604907497833
Abcg1	3060	4800	1.569	0.65	2.39080373574238e-5	0.00739417886409428
Adk	420	826	1.963	0.973	4.11208870821991e-8	2.95050588992195e-5
Arhgap5	566	959	1.699	0.765	1.4598619356449e-4	0.0311750040495237
Atp6v0c-ps2	20	182	9.124	3.19	9.38486254275277e-16	1.5304151299263598e-12
Ctse	744	4444	5.974	2.579	9.73537288912741e-73	8.731655944258379e-69
Ctso	1906	3132	1.644	0.717	6.89995361480135e-8	4.58412473860395e-5
Cxcr4	16384	24590	1.501	0.586	4.17674973187954e-7	2.4974178896818e-4
Cyp27a1	312	640	2.054	1.038	1.96906125445597e-7	1.2179662338769e-4
D16Ertd472e	1156	2074	1.793	0.843	2.612311866037e-8	1.95248542720715e-5
Dnah8	799	2186	2.732	1.45	1.4451414451258602e-15	2.16024560355564e-12
Dyrk3	286	494	1.726	0.787	1.2085893782092e-4	0.026765032427553
Eya1	342	653	1.908	0.932	7.95376312710286e-7	4.1025024564626e-4
Gnb4	118	354	2.987	1.579	3.95858213616336e-10	3.38138315992849e-7
Hdac9	2135	3452	1.616	0.693	3.56503696134364e-6	0.00155974714664835
Hepacam2	320	894	2.793	1.482	4.3377055635727397e-13	4.57704484702164e-10
Hmga1b	7	153	22.761	4.508	3.91084462440521e-16	7.62067242546415e-13
Igha	843	2421	2.873	1.522	9.67511091545799e-28	4.33880349003714e-24
Ighg2b	593	1632	2.755	1.462	5.56283808835061e-20	1.42551699469762e-16
Ighg2c	317	1088	3.437	1.781	5.3227352877163604e-14	5.967451599441e-11
Igkv6-17	500	810	1.621	0.697	2.5144335575027e-4	0.0475590988698733
Islr2	90	264	2.914	1.543	1.48135847141786e-7	9.490217235819l6e-5
Kcnh6	4	150	32.902	5.04	1.8605303978737203e-15	2.56724571361991e-12
Kif18a	1568	2579	1.644	0.717	1.17474921008283e-6	5.6953111703961e-4
Klf4	7503	11306	1.507	0.592	1.3516880439727e-4	0.0295690001619308
Lgals3	174	333	1.922	0.943	5.29357234601036e-5	0.013761753730831
Lmna	1108	1801	1.625	0.701	4.32716357675586e-5	0.0115851731701264
Ltk	402	796	1.988	0.991	5.94914869933211e-6	0.00231990933410042
Myadm	1032	3292	3.191	1.674	8.2306343006773e-32	4.92137060285164e-28
Nampt	7695	16368	2.127	1.089	4.19944119758951e-14	5.02197174682404e-11
Nap1l3	26	99	3.732	1.9	2.07392020698267e-5	0.00664321083443843
Nrip1	1115	2313	2.075	1.053	1.38316010726254e-12	1.3783958891153e-9
P2ry10	12306	18726	1.522	0.606	4.21001126677799e-5	0.0114971040042835
Pira2	42	137	3.234	1.693	9.55066224216315e-6	0.00335921135882201
Prf1	227	446	1.966	0.975	5.33331082939172e-6	0.0021742938558552
Prkca	721	1170	1.622	0.698	3.90387775650536e-5	0.0109418373744052
Prkcg	205	522	2.537	1.343	1.64034911064582e-10	1.47122911733823e-7
Prss41	4	48	11.615	3.538	7.99628982718875e-6	0.00298828014416899
Rfk	2376	3687	1.552	0.634	5.89754438873763e-7	3.2057621589447e-4
Rgcc	864	1410	1.634	0.708	1.4458483240162e-4	0.0311750040495237
Rnps1-ps	16	164	10.114	3.338	2.23727544966743e-15	2.86658907258102e-12
Ryr2	448	3638	8.133	3.024	5.54885820139486e-101	9.953541841662109e-97
Sestd1	19	110	5.761	2.526	5.04666230844608e-8	3.48180878803484e-5
Sgk3	1817	2748	1.513	0.598	2.29052817756475e-5	0.00720833235950115
Spp1	130	268	2.053	1.037	6.14590493314083e-5	0.0154680295637212
Stt3b	4927	8259	1.676	0.745	2.81046981964686e-9	2.29155489203752e-6
Sult2b1	15	73	4.733	2.243	3.12371572585334e-5	0.00889416074450114
Syne1	2812	5927	2.108	1.076	1.65526094327379e-16	3.71150885005564e-13
Tagap1	896	2046	2.284	1.191	4.24834007440303e-16	7.62067242546415e-13
Thnsl1	304	508	1.676	0.745	2.51873920874e-4	0.0475590988698733
Uchl3	1342	2130	1.587	0.666	4.79346376607084e-5	0.012644875446438
Zfp619	312	564	1.805	0.852	3.07741978779807e-5	0.00889416074450114

Supplementary Table S5: List of differentially expressed genes in in vitro-activated B cells (day 2)

Genes downregulated in LPS activated B cells (Day2)						
MGI SYMBOL	**WT**	**cKO**	**FoldChange**	**log2FoldChange**	**pvalue**	**padj**
Tbc1d23	1493	992	0.665	-0.589	1.4379663512243e-4	0.0154285330860781
Igf2bp3	316	179	0.567	-0.818	1.9768790415222e-4	0.018342053761529
St6galnac2	442	246	0.557	-0.844	2.261740315660037e-5	0.00352169516467702
Oasl1	9256	4244	0.458	-1.125	9.28749197296647e-37	1.97637829184726e-33
BC018473	1640	689	0.421	-1.25	4.44834189667717e-19	5.67964293367741e-16

Genes upregulated in LPS activated B cells (Day2)						
MGI SYMBOL	**WT**	**cKO**	**FoldChange**	**log2FoldChange**	**pvalue**	**padj**
Apoe	298	540	1.816	0.861	1.81573739597255e-5	0.00289791688397219
Arhgap31	16	64	4.088	2.031	1.9870840560962e-4	0.018342053761529
Ctse	162	1482	9.113	3.188	1.57292762828546e-82	5.0207849894871706e-79
Gdpd3	248	444	1.796	0.844	4.9041339772894e-4	0.0361942096081108
Gnb4	221	393	1.776	0.829	1.9871185085713e-4	0.018342053761529
Hepacam2	313	606	1.944	0.959	4.49632763275736e-6	9.4113297073845e-4
Igha	83	176	2.12	1.084	3.6973674915831e-4	0.0289619559095296
Ighv1-12	361	714	1.986	0.99	5.06951090721622e-7	1.4710798923485e-4
Ighv1-15	1508	2324	1.541	0.624	7.40335530853516e-8	2.70074401655363e-5
Ighv1-4	493	899	1.825	0.868	3.53546764360655e-8	1.41065158979901e-5
Ighv1-5	324	606	1.874	0.906	4.0459821172115e-6	8.609849945426e-4
Ighv1-59	574	876	1.525	0.608	2.9926435400817e-4	0.0248117355323144
Ighv1-63	144	269	1.869	0.902	5.9253469477392e-4	0.0414736629072173
Ighv1-64	2602	3972	1.527	0.611	1.8496408629221902e-9	1.18081072688953e-6
Ighv1-66	538	838	1.558	0.64	1.26166319526729e-5	0.0022067007776949
Ighv1-72	1966	2973	1.513	0.597	2.40844660273244e-6	5.3949203901206e-4
Ighv1-74	523	948	1.813	0.858	1.22429770556603e-8	6.51326379361127e-6
Ighv1-75	1150	1776	1.546	0.628	4.81417058761007e-9	2.67249261141762e-6
Ighv1-78	734	1161	1.585	0.664	5.53927069622126e-5	0.00693386355385815
Ighv1-81	1140	1819	1.595	0.674	1.72190560641577e-8	8.34493367916676e-6
Ighv2-9-1	620	977	1.576	0.657	1.61387954854543e-5	0.00267610572413351
Ighv4-1	471	708	1.503	0.588	3.3048049394524e-4	0.0263723434168308
Ighv5-12	371	598	1.615	0.692	1.6879600372217e-4	0.0171046617105132
Ighv5-16	1089	2268	2.084	1.059	4.77433382396421e-13	4.68913032802885e-10
Ighv5-9-1	660	1096	1.661	0.732	3.49389624702796e-5	0.00474575183851628
Ighv7-1	268	586	2.192	1.132	8.74210264846859e-8	3.01984854471224e-5
Ighv8-12	1012	1624	1.605	0.682	5.79361119675743e-7	1.5738899523446e-4
Igkv15-103	884	1446	1.637	0.711	1.22433311217471e-5	0.00217115071892316
Igkv17-121	1697	2604	1.534	0.618	1.13783903477559e-6	2.8486134894146e-4
Igkv17-127	2162	3536	1.636	0.71	6.573807157500919e-11	4.93731586982187e-8
Igkv3-12	1044	1871	1.793	0.842	3.83146231752191e-9	2.22364140318726e-6
Igkv3-7	706	1224	1.734	0.794	2.8455666007439504e-9	1.73010449325232e-6
Igkv4-55	876	1326	1.512	0.597	6.54042596310273e-6	0.00128474090302916
Igkv4-57	1073	2028	1.891	0.919	3.3562498027467997e-12	2.8568398320980804e-9
Igkv4-57-1	442	742	1.682	0.75	7.75445977469986e-6	0.00147774540900549
Igkv4-59	1852	2888	1.56	0.641	4.83655880379133e-8	1.81627008255317e-5
Igkv4-61	202	382	1.895	0.922	1.60994968749444e-5	0.00267610572413351
Igkv4-63	412	664	1.612	0.689	9.0568117075039907e-005	0.0103247653465545
Igkv4-68	765	1308	1.711	0.775	7.69625556942995e-7	2.0054243083771e-4
Igkv5-39	1219	2002	1.643	0.717	1.26271126979818e-7	4.13392243404698e-5
Igkv5-45	468	718	1.533	0.616	5.9442984899912e-4	0.0414736629072173
Igkv5-48	1414	2136	1.51	0.594	1.50238092173931e-7	4.79559990219186e-5
Igkv6-13	486	748	1.539	0.622	3.57710546180523e-5	0.00480762974066624
Igkv6-14	122	282	2.299	1.201	5.46043365617278e-7	1.5493070427114e-4
Igkv6-15	2835	4390	1.549	0.632	1.85196308197933e-8	8.34493367916676e-6
Igkv6-17	1384	2542	1.837	0.877	8.67158226982118e-14	1.00653420382797e-10
Igkv6-23	1326	2087	1.575	0.655	8.75112751835471e-8	3.01984854471224e-5
Igkv6-25	514	814	1.582	0.661	3.15389222964394e-5	0.00442515340528504
Igkv8-19	1282	1964	1.532	0.616	6.14025172420464e-6	0.00122498021897883
Igkv8-21	657	1012	1.542	0.625	5.52356193294069e-5	0.00693386355385815
Il9r	221	524	2.371	1.245	1.0811900504023099e-11	8.6278966022104e-9
Lax1	2834	4282	1.511	0.596	4.67891232373424e-7	1.3893105244055e-4
Maged1	292	498	1.708	0.773	1.65786385160679e-5	0.00271379559709174
Myadm	164	371	2.254	1.173	4.74959906327652e-8	1.81627008255317e-5
Oasl2	72	588	8.259	3.046	6.047550256581949e-45	1.54430243352077e-41
Pde8a	537	848	1.58	0.66	1.0115348773303e-5	0.00189930548731666
Pon3	561	854	1.524	0.608	4.2294877988406e-4	0.0323365869554472
Prdm16	234	400	1.71	0.774	8.25736604363825e-5	0.00949820267073632
Ryr2	78	296	3.798	1.925	2.64953991271621e-13	2.81911046713004e-10
Selplg	1664	2546	1.53	0.614	1.85267444878709e-8	8.34493367916676e-6
Sord	515	775	1.502	0.587	2.2488993993367e-4	0.0199402413407862
Spp1	86	228	2.622	1.391	1.55222797931981e-6	3.8113166999914e-4
Tram2	646	982	1.52	0.604	7.25890543153912e-5	0.00858163931017513
Ubc	3298	5570	1.688	0.756	9.853193214380549e-20	1.39783967734679e-16

Supplementary Table S6: List of differentially expressed genes in in vitro-differentiated plasmablasts (day 4)

Genes upregulated in plasmablasts (Day4)						
MGI SYMBOL	**WT**	**cKO**	**FoldChange**	**log2FoldChange**	**pvalue**	**padj**
Iglv3	18404	38273	2.079	1.056	1.79921733414964e-12	2.31613247425083e-8
Rps7-ps3	1038	2096	2.02	1.015	4.144740942877341e-9	1.3338812539415e-5
Ighv3-8	6327	11801	1.865	0.899	2.16216554785762e-5	0.0397622244251016
Reep5	3030	5507	1.817	0.861	3.29776904916066e-5	0.0471690899664946
Glb1	1322	2165	1.638	0.712	3.02476519318689e-5	0.0471690899664946
Atf5	412	745	1.805	0.852	3.71673509239989e-5	0.0478455308444638

Supplementary Table S7: Total number of mutations, total number of bp analyzed and mutation frequencies within intron 5' to Sμ (A, B); 3' to J_H4 (C, D) and 3' to J_K5 (E, F) in GC B cells of wt and Satb1 cKO. For each region tested for SHM, data were obtained from spontaneous GC B cells sorted from Peyer's patches (n=6-9 individual mice) or splenic GC B cells sorted upon NP-CGG-immunization (n=7-8 individual mice).

S7A

Intron 5' to Smu Peyer's patches GC							
Satb1$^{flx/+}$				Satb1$^{flx/flx}$ Cd79a$^{cre/+}$			
N°	number of mutations	total number of pb analyzed	Frequency (mutation/Kb)	N°	number of mutation	total number of pb analyzed	Frequency (mutation/Kb)
8692	167 611	143 504 465	**1,17**	**8690**	151 915	100 956 853	**1,50**
8649	45 504	48 022 564	**0,95**	**8645**	54 050	38 428 176	**1,40**
8753	143 998	96 361 943	**1,50**	**8756**	311 660	148 421 088	**2,10**
8755	182 738	122 821 454	**1,49**	**9601**	144 996	73 409 771	**1,98**
8644	109 695	63 612 833	**1,72**	**9604**	163 545	78 032 498	**2,10**
7128	250 366	152 000 328	**1,65**	**9877**	162 887	85 164 912	**1,91**
7129	176 860	139 941 043	**1,26**	**9880**	113 784	87 909 626	**1,29**
9881	152 289	86 749 376	**1,76**	**7111**	485 120	187 778 619	**2,58**
				7112	252 555	121 402 038	**2,08**
Total	1 229 061	853 014 006	**1,44**	**Total**	1 840 512	921 503 581	**1,88**

S7B

Intron 5' to Smu NP CGG Splenic GC							
Satb1$^{flx/+}$				Satb1$^{flx/flx}$ Cd79a$^{cre/+}$			
N°	number of mutations	total number of pb analyzed	Frequency (mutation/Kb)	N°	number of mutation	total number of pb analyzed	Frequency (mutation/Kb)
8139	19 700	111 850 026	**0,18**	**6854**	26 279	142 403 067	**0,19**
6858	48 673	211 877 661	**0,23**	**6857**	56 795	146 983 925	**0,39**
6859	8 202	129 181 296	**0,06**	**6864**	30 662	52 155 066	**0,59**
6863	7 520	132 861 196	**0,06**	**6687**	106 971	229 058 581	**0,47**
6692	25 891	179 825 690	**0,14**	**6691**	101 092	256 700 586	**0,39**
6693	109 022	217 449 208	**0,50**	**6791**	33 527	118 595 323	**0,28**
2544	67 300	178 614 933	**0,38**	**2537**	112 115	197 775 331	**0,57**
Total	286 308	1 161 660 010	**0,22**	**Total**	467 441	1 143 671 879	**0,41**

S7C

Intron 3' to J_H4 Peyer's patches GC							
$Satb1^{flx/+}$				$Satb1^{flx/flx}$ $Cd79a^{cre/+}$			
N°	number of mutations	total number of pb analyzed	Frequency (mutation/Kb)	N°	number of mutation	total number of pb analyzed	Frequency (mutation/Kb)
8692	57 561	7 906 004	**7,28**	**8690**	621 327	82 879 451	**7,50**
8649	654 842	100 297 965	**6,53**	**8645**	328 574	32 909 115	**9,98**
8753	4 064 096	339 723 680	**11,96**	**8756**	106 623	13 743 216	**7,76**
8755	218 499	26 244 087	**8,33**	**9601**	1 718 084	140 896 971	**12,19**
8644	136 754	10 382 456	**13,17**	**9604**	1 866 361	127 867 165	**14,60**
8646	475 950	58 858 803	**8,09**	**9605**	2 112 619	142 861 789	**14,79**
9881	195 215	21 355 525	**9,14**	**9661**	2 550 716	146 382 941	**17,42**
				9877	757 522	57 471 525	**13,18**
				9880	1 614 250	119 121 342	**13,55**
Total	5 802 917	564 768 520	**9,21**	**Total**	10 061 826	745 012 173	**12,33**

S7D

Intron 3' to J_H4 NP CGG Splenic GC							
$Satb1^{flx/+}$				$Satb1^{flx/flx}$ $Cd79a^{cre/+}$			
N°	number of mutations	total number of pb analyzed	Frequency (mutation/Kb)	N°	number of mutation	total number of pb analyzed	Frequency (mutation/Kb)
8139	152 171	39 872 610	**3,81**	**8133**	137 111	28 459 587	**4,82**
6858	84 367	38 653 923	**2,18**	**6854**	252 934	92 925 446	**2,72**
6859	125 264	78 908 567	**1,59**	**6857**	141 510	37 358 940	**3,79**
6863	153 921	58 613 945	**2,62**	**6864**	335 616	40 332 921	**8,32**
6692	317 757	68 343 790	**4,65**	**6687**	777 955	152 063 704	**5,12**
6693	270 476	59 540 608	**4,55**	**6691**	551 228	96 233 795	**5,73**
2544	151 910	41 648 331	**3,64**	**6791**	249 260	54 111 722	**4,61**
				2537	176 658	32 694 946	**5,40**
Total	1 255 866	385 581 774	**3,29**	**Total**	2 622 272	534 181 061	**5,06**
Total	1 255 866	385 581 774	**3,29**	**Total**	2 622 272	534 181 061	**5,06**

S7E

Intron 3' to Jk5 Peyer's patches GC							
Satb1$^{flx/+}$				Satb1$^{flx/flx}$ Cd79a$^{cre/+}$			
N°	number of mutations	total number of pb analyzed	Frequency (mutation/Kb)	N°	number of mutation	total number of pb analyzed	Frequency (mutation/Kb)
8692	64 352	8 109 925	**7,94**	**8690**	977 250	109 513 034	**8,92**
8649	187 594	18 973 865	**9,89**	**8645**	133 351	11 622 636	**11,47**
8753	41 647	2 737 783	**15,21**	**8756**	1 092 197	76 790 583	**14,22**
8755	2 497 183	288 443 955	**8,66**	**9601**	1 097 124	100 505 774	**10,91**
8644	400 715	30 094 611	**13,32**	**9604**	1 941 371	110 394 569	**17,59**
9881	958 245	97 655 675	**9,81**	**9605**	779 895	62 212 383	**12,54**
7128	1 571 163	146 409 208	**10,73**	**9877**	820 899	65 692 001	**12,50**
7129	540 065	97 174 751	**5,56**	**9880**	2 136 606	163 662 781	**13,05**
				7111	963 266	90 045 963	**10,70**
				7112	1 256 410	223 536 225	**6,07**
Total	6 260 964	689 599 773	**10,14**	**Total**	6 842 087	536 730 980	**11,80**

S7F

Intron 3' to Jk5 NP CGG Splenic GC							
Satb1$^{flx/+}$				Satb1$^{flx/flx}$ Cd79a$^{cre/+}$			
N°	number of mutations	total number of pb analyzed	Frequency (mutation/Kb)	N°	number of mutation	total number of pb analyzed	Frequency (mutation/Kb)
8139	222 655	85 014 498	**2,62**	**6854**	171 154	69 778 869	**2,45**
6858	72 960	56 300 498	**1,30**	**6857**	271 677	110 895 960	**2,45**
6859	2 008	1 253 443	**1,60**	**6864**	280 371	67 161 110	**4,16**
6863	121 103	93 266 492	**1,30**	**6687**	371 949	94 961 964	**3,92**
6692	196 340	96 679 417	**2,03**	**6691**	249 263	71 580 665	**3,48**
6693	323 874	88 558 220	**3,66**	**6791**	247 551	102 051 591	**2,43**
2544	731 196	178 302 885	**4,10**	**2537**	622 428	91 007 705	**6,84**
Total	1 670 136	599 375 453	**2,37**	**Total**	2 214 393	607 437 864	**3,68**